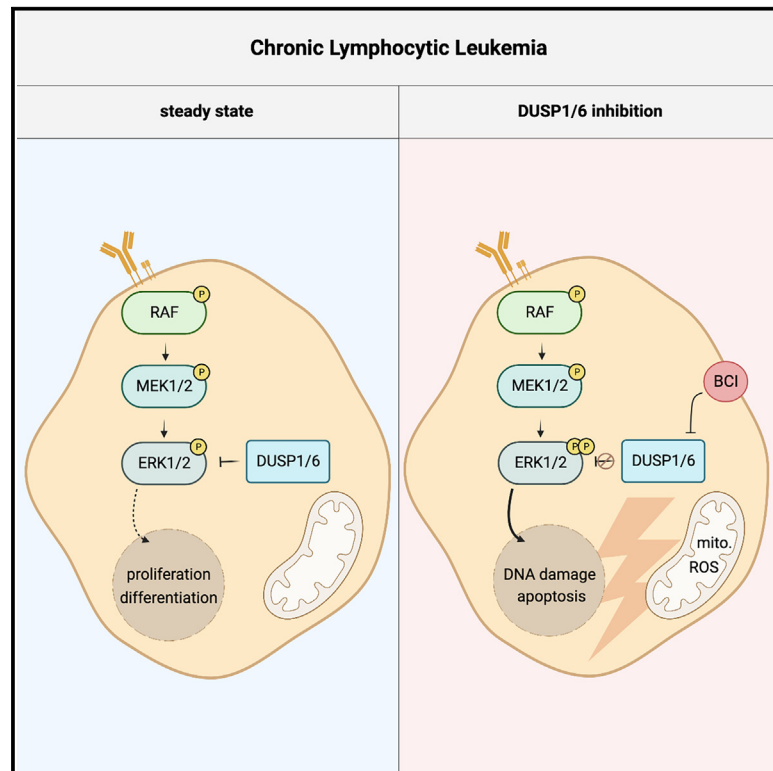


## Negative feedback regulation of MAPK signaling is an important driver of chronic lymphocytic leukemia progression

### Graphical abstract



### Authors

Veronika Ecker, Lisa Brandmeier, Martina Stumpf, ..., Julia Jellusova, Jürgen Ruland, Maike Buchner

### Correspondence

maike.buchner@tum.de

### In brief

Ecker et al. show that targeting DUSP1/6, negative regulators, induces overwhelming intracellular signaling, causing harmful mitochondrial ROS accumulation in CLL cells. This leads to DNA damage and apoptotic CLL cell death. Their findings propose DUSP1/6 inhibition as a potential treatment strategy, even for drug-resistant CLL.

### Highlights

- DUSP1/6 inhibition in CLL triggers rapid MAPK signaling and cell death
- Enhanced MAPK signaling leads to mitochondrial ROS accumulation
- This ROS accumulation leads to DNA damage and subsequent CLL cell apoptosis
- DUSP1/6 inhibition is highly effective against treatment-resistant CLL



## Article

# Negative feedback regulation of MAPK signaling is an important driver of chronic lymphocytic leukemia progression

Veronika Ecker,<sup>1,2,17</sup> Lisa Brandmeier,<sup>1,2,17</sup> Martina Stumpf,<sup>1,2</sup> Piero Giansanti,<sup>2,3,4</sup> Aida Varela Moreira,<sup>5</sup> Lisa Pfeuffer,<sup>1,2</sup> Marcel H.A.M. Fens,<sup>5,6</sup> Junyan Lu,<sup>7</sup> Bernhard Kuster,<sup>3,4,8,9</sup> Thomas Engleitner,<sup>2,10</sup> Simon Heidegger,<sup>2,11</sup> Roland Rad,<sup>2,8,10</sup> Ingo Ringshausen,<sup>12</sup> Thorsten Zenz,<sup>13</sup> Clemens-Martin Wendtner,<sup>14</sup> Markus Müschen,<sup>15</sup> Julia Jellusova,<sup>1,2</sup> Jürgen Ruland,<sup>1,2,8,9,16</sup> and Maïke Buchner<sup>1,2,18,\*</sup>

<sup>1</sup>Institute of Clinical Chemistry and Pathobiochemistry, School of Medicine, Technical University of Munich, Munich, Germany

<sup>2</sup>TranslaTUM - Central Institute for Translational Cancer Research, Technische Universität München, 81675 Munich, Germany

<sup>3</sup>Chair of Proteomics and Bioanalytics, Technical University of Munich (TUM), Freising, Bavaria, Germany

<sup>4</sup>Bavarian Center for Biomolecular Mass Spectrometry at the University hospital rechts der Isar (BayBioMS@MRI), Technical University of Munich, Munich, Germany

<sup>5</sup>Department of Clinical Chemistry and Haematology, University Medical Center Utrecht, Utrecht, the Netherlands

<sup>6</sup>Department of Pharmaceuticals, Utrecht Institute for Pharmaceutical Sciences, Utrecht University, Utrecht, the Netherlands

<sup>7</sup>European Molecular Biology Laboratory (EMBL), Heidelberg, Germany

<sup>8</sup>German Cancer Consortium (DKTK), Munich Partner Site, Munich, Germany

<sup>9</sup>German Cancer Research Center (DKFZ), Heidelberg, Germany

<sup>10</sup>Institute of Molecular Oncology and Functional Genomics, TUM School of Medicine, Technical University of Munich, 81675 Munich, Germany

<sup>11</sup>Department of Medicine III, School of Medicine, Technical University of Munich, Munich, Germany

<sup>12</sup>Wellcome Trust/MRC Cambridge Stem Cell Institute and Department of Haematology, Jeffrey Cheah Biomedical Centre, University of Cambridge, Cambridge CB2 0AH, UK

<sup>13</sup>Department of Medical Oncology and Hematology, University Hospital and University of Zurich, 8091 Zurich, Switzerland

<sup>14</sup>Munich Clinic Schwabing, Academic Teaching Hospital, Ludwig-Maximilian University (LMU), Munich, Germany

<sup>15</sup>Center of Molecular and Cellular Oncology, Yale School of Medicine, 300 George Street, New Haven, CT 06520, USA

<sup>16</sup>German Center for Infection Research (DZIF), Partner Site Munich, Munich, Germany

<sup>17</sup>These authors contributed equally

<sup>18</sup>Lead contact

\*Correspondence: [maike.buchner@tum.de](mailto:maike.buchner@tum.de)  
<https://doi.org/10.1016/j.celrep.2023.113017>

## SUMMARY

Despite available targeted treatments for the disease, drug-resistant chronic lymphocytic leukemia (CLL) poses a clinical challenge. The objective of this study is to examine whether the dual-specific phosphatases DUSP1 and DUSP6 are required to negatively regulate mitogen-activated protein kinases (MAPKs) and thus counterbalance excessive MAPK activity. We show that high expression of DUSP6 in CLL correlates with poor clinical prognosis. Importantly, genetic deletion of the inhibitory phosphatase DUSP1 or DUSP6 and blocking DUSP1/6 function using a small-molecule inhibitor reduces CLL cell survival *in vitro* and *in vivo*. Using global phospho-proteome approaches, we observe acute activation of MAPK signaling by DUSP1/6 inhibition. This promotes accumulation of mitochondrial reactive oxygen species and, thereby, DNA damage and apoptotic cell death in CLL cells. Finally, we observe that DUSP1/6 inhibition is particularly effective against treatment-resistant CLL and therefore suggest transient DUSP1/6 inhibition as a promising treatment concept to eliminate drug-resistant CLL cells.

## INTRODUCTION

Chronic lymphocytic leukemia (CLL) is among the most frequent B cell malignancies in the Western world and is characterized by clonal accumulation of mature CD5-positive B cells. Signaling from the B cell receptor (BCR) plays a significant role in promoting CLL pathogenesis.<sup>1–4</sup> Inhibiting BCR downstream effectors with the Bruton's tyrosine kinase (BTK) inhibitor ibrutinib, among

others, is highly effective in lowering the disease burden and has transformed CLL therapy in recent years. Despite these targeted therapies, CLL remains an incurable disease for most patients, and the emergence of drug-resistant CLL demands the exploration of alternative treatments.<sup>5</sup>

Activation of the mitogen-activated protein kinase (MAPK) pathway promotes CLL cell proliferation and survival and occurs downstream of surface receptors, including the BCR. In addition,



the MAPK signaling pathway is frequently activated by mutations in CLL, with 8.7% of patients carrying at least one mutation in MAPK pathway genes such as NRAS, KRAS, and BRAF.<sup>6</sup> Importantly, patients with MAPK-activating mutations in CLL comprise a distinct subgroup with poor clinical characteristics such as shorter treatment-free survival<sup>7,8</sup> and higher drug resistance.<sup>9–11</sup> However, clinical studies of FDA-approved MEK or BRAF inhibitors for CLL have yielded poor outcomes.<sup>12</sup> As a result, despite its importance in CLL etiology, elevated MAPK signaling is yet to be addressed therapeutically.

The physiological outcome of MAPK signaling in B cells varies greatly depending on the maturation stage and activation status.<sup>13</sup> ERK1/2 activation, for example, is predominantly known for its pro-survival effects. However, depending on the duration, the magnitude and its subcellular localization, ERK1/2 activation can also trigger apoptotic processes, particularly upon treatment with DNA-damaging agents, such as etoposide,<sup>14</sup> but also upon CD40 ligation in B cell lymphoma.<sup>15</sup> Physiologically, ERK-induced cell death is particularly important in developing B cells when autoreactive B cells are eliminated.<sup>16,17</sup> Thus, the actual role of MAPK activation is highly cell and context dependent. MAPK is negatively regulated by the expression of dual-specificity protein phosphatases (DUSPs), which specifically dephosphorylate phospho-threonine and -tyrosine residues that activate MAPKs. Two distinct members of the DUSP family, DUSP1 and DUSP6, inactivate ERK1/2 by dephosphorylation. Although DUSP6 is specific for ERK1/2, DUSP1 also dephosphorylates JNK and p38. Both DUSPs are dysregulated in various diseases, including cancer. They can either function as tumor suppressors by inhibiting ERK activation<sup>18,19</sup> or as oncogenes by assisting tumor cells in adapting to high levels of MAPK signaling.<sup>20,21</sup> Although adaptation to signaling levels is critical for a number of B cell malignancies,<sup>21</sup> the role of MAPK-negative feedback via the DUSP family in CLL remains largely unknown.

In the present study, we explored the importance of DUSP1- and DUSP6-mediated negative regulation of MAPK in CLL and identified DUSP6 overexpression as a marker of enhanced MAPK activity and, hence, poor clinical prognosis in CLL. We showed that DUSP1 and DUSP6 are necessary in CLL to avoid apoptosis via the DNA damage response pathway by counterbalancing excessive oncogenic MAPK activation. Therefore, the inhibition of DUSP1 and DUSP6 significantly reduced the CLL burden in preclinical models and was highly effective in the treatment of drug-resistant CLL.

## RESULTS

### Expression of the MAPK-negative regulator DUSP6 but not DUSP1 is associated with poor clinical prognosis in CLL and may reflect ERK activity

To investigate the potential role of negative feedback regulation of MAPK signaling in CLL, we first analyzed the mRNA expression levels of DUSP1 and DUSP6 in a total number of 210 CLL samples.<sup>22</sup> We observed that both DUSP1 and DUSP6 were readily expressed in all tested CLL samples, with higher levels of DUSP6 and lower levels of DUSP1 in CLL cases carrying unmutated BCRs, which is one of the strongest predictive factors for poor disease outcome (Figures 1A and 1B). We also evaluated whether

DUSP1 and DUSP6 expression is associated with CLL prognosis. We correlated the mRNA expression levels of DUSP1 and DUSP6 with time to treatment (TTT) and overall survival (OS).<sup>22,23</sup> DUSP1 expression was not associated with clinical parameters (Figures S1A and S1B), and we found that high expression of DUSP6 in CLL samples was associated with adverse clinical outcomes, indicated by decreased TTT (Figure 1C) and OS (Figure 1D). Analysis of DUSP6 expression in the mutated or unmutated CLL subsets indicated that high DUSP6 levels are only significantly associated with shorter TTT in the mutated CLL subset, which could be due to the limited number of patients analyzed (Figure S1C). However, we noticed that CLL samples with mutations in the KRAS and BRAF genes (causing high levels of MAPK signaling) expressed very high levels of DUSP6 (Figure 1E). However, this was not the case when we compared DUSP1 levels in CLL samples with KRAS and BRAF mutations (Figure S1D). Notably, DUSP6 expression is not an independent risk factor. High DUSP6 expression rather indicates CLL samples with high levels of MAPK signaling, regardless of whether these are derived from the active BCR signaling in unmutated CLL cases or via activating mutations within the MAPK pathway itself.

As negative regulators are commonly induced in response to stimulation,<sup>25,26</sup> we hypothesized that the levels of DUSP6 in CLL cells are directly related to the degree of MAPK signaling.<sup>27</sup> To test whether MAPK signaling affects DUSP6 expression levels, we reanalyzed a published transcriptional dataset of CLL samples treated with the MEK1/2 inhibitor selumetinib.<sup>23</sup> In addition to the expected downregulation of the transcription factors EGR1 and EGR2, which participate in the proliferative response of CLL cells upon BCR ligation,<sup>28</sup> we observed strong downregulation of the negative feedback molecule DUSP6 upon MAPK pathway inhibition in CLL (Figure 1F). Furthermore, we confirmed this finding using the MEK inhibitor PD0325901 (PD901) and DUSP6 protein levels, in conjunction with reduced ERK phosphorylation (Figures 1G and 1H). Stimulation of CLL cells by microenvironmental factors engages the BCR and MAPK signaling pathways in CLL cells, so we also analyzed DUSP6 expression in matched samples collected from the peripheral blood and lymph nodes using publicly available data.<sup>24</sup> Indeed, DUSP6 and DUSP1 expression was higher in lymph node-derived CLL cells than in the respective peripheral blood CLL samples (Figures 1I and 1J). Taken together, we conclude that the MAPK-negative regulators DUSP1 and DUSP6 are commonly expressed in CLL and are dynamically upregulated in response to microenvironmental stimulation. High levels of DUSP6 expression, but not DUSP1 expression, define a subset of patients with poor prognosis, particularly those with KRAS and BRAF mutations.

### DUSP1/6 inhibition is toxic specifically for CLL cells

To investigate the functional relevance of DUSP1- and DUSP6-mediated negative MAPK regulation in CLL, we tested the effects of the DUSP1/6-specific small-molecule inhibitor BCI<sup>29</sup> on CLL cells. We treated 21 primary CLL samples harvested from the peripheral blood of patients for 48 h with increasing doses of BCI and found a dose-dependent induction of specific cell death *in vitro* (Figure 2A). We calculated the specific cell death in vehicle-treated control CLL cells undergoing

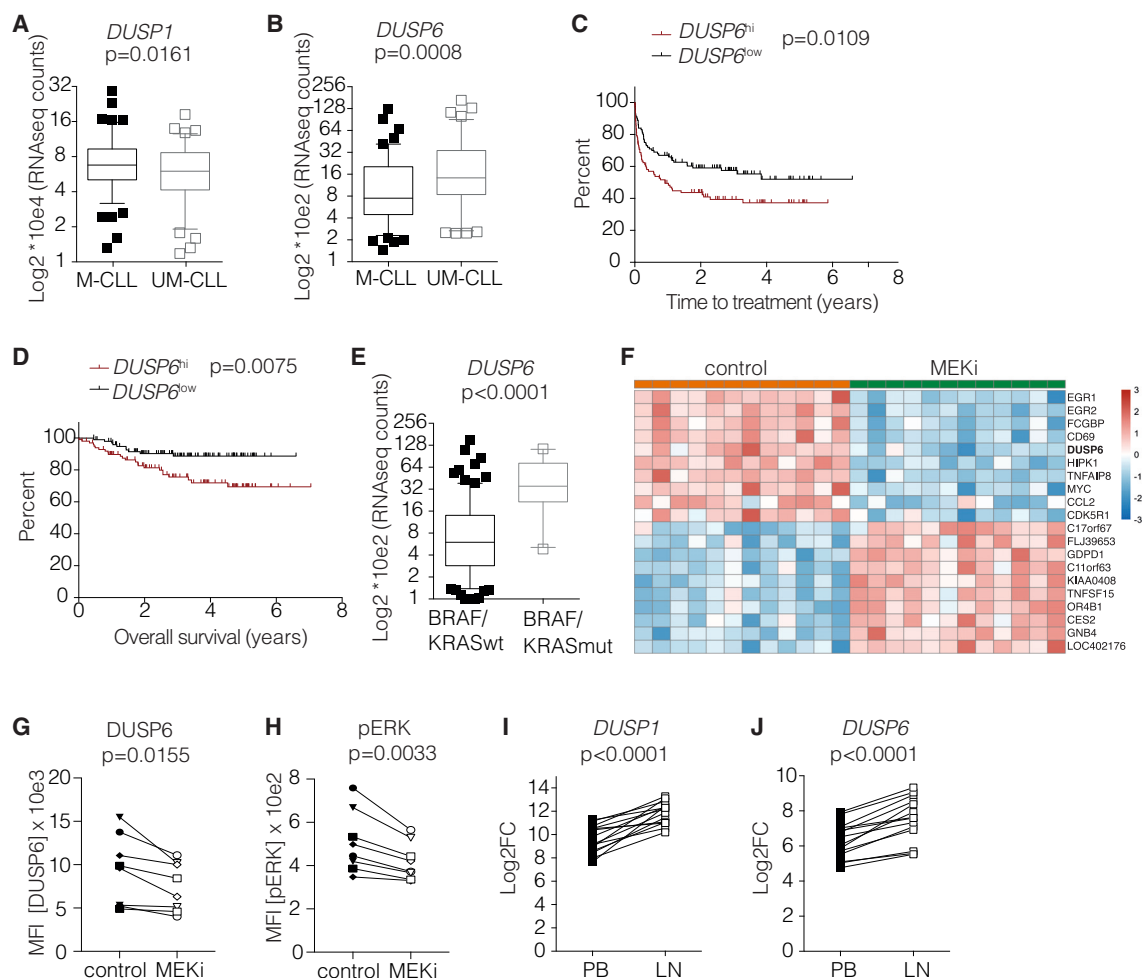


**Figure 1. The MAPK-negative regulator DUSP6 but not DUSP1 expression is associated with poor clinical prognosis in CLL and may reflect ERK activity**

(A and B) RNAseq counts of DUSP1 mRNA (A) and DUSP6 mRNA (B) in IGVH-mutated (M-CLL;  $n = 94$ ) compared to IGVH-unmutated (UM-CLL;  $n = 95$ ) CLL patient-derived samples. CLL cells were obtained from the peripheral blood. Data are presented as  $\log_2 \times 10^4$  values  $\pm$  SD. Statistical significance was assessed by a two-tailed unpaired Student's  $t$  test (DUSP1  $p = 0.0161$ ; DUSP6  $p = 0.0008$ ).<sup>23</sup>

(C and D) Correlation of mRNA expression levels of DUSP6 in CLL samples (C) ( $n = 210$ ). DUSP6 high and DUSP6 low samples (defined by above or below the median expression level) were displayed as time to treatment (TTT) curve ( $p = 0.0109$ ) and (D) overall survival (OS) curve ( $p = 0.0075$ ).<sup>23</sup> Statistical analysis was performed using the log rank (Mantle Cox) test.

(E) RNA-seq counts of DUSP6 mRNA in CLL samples with mutated BRAF and KRAS genes. Comparison of KRAS/BRAF wild-type (wt;  $n = 189$ ) compared to KRAS/BRAF mutation ( $n = 21$ ). Data are presented as  $\log_2 \times 10^4$  values  $\pm$  SD. Statistical significance was assessed by a two-tailed unpaired Student's  $t$  test (DUSP6  $p < 0.0001$ ).

(F) Transcriptional analysis upon MEK inhibition in CLL samples revealed DUSP6 among the top downregulated genes compared to the vehicle control in a published dataset.<sup>23</sup>

(G and H) Analysis of the DUSP6 protein levels (G) and corresponding phospho-ERK mean fluorescence intensity (MFI) (H) of 2 CLL-derived cell lines with 2 sublines (transduced with the Eco receptor and cultured separately) treated with 5  $\mu$ M MEK inhibitor (PD901) for 24 h ( $n = 4$ , pooled data from 2 independent experiments) ( $\blacklozenge$ , OSU-CLL;  $\bullet$ , MEC-1;  $\blacksquare$ , OSU-CLL Eco;  $\blacktriangledown$ , MEC-1 Eco). Statistical significance was assessed by a two-tailed paired Student's  $t$  test (DUSP6  $p < 0.0155$ ) (pERK  $p < 0.0033$ ).

(I and J) Comparison of reanalyzed gene expression publicly available data<sup>24</sup> of (I) DUSP1 expression ( $n = 14$ ;  $p < 0.0001$ ) and (J) DUSP6 expression ( $n = 14$ ;  $p < 0.0001$ ) specified as  $\log_2$  fold change (logFC) in matched peripheral blood samples and lymph node samples.

spontaneous apoptosis in cell culture.<sup>30</sup> Absolute viability of the samples is depicted in Figure S1E. There was no significant difference in the response of CLL to BCI based on the mutational status of their BCR (Figure S1F). In addition, cell death was specifically induced in CLL cells, whereas B cells derived from healthy donors remained largely unaffected by DUSP1/6 inhibi-

tion at the tested concentrations (Figure 2B). Furthermore, we confirmed the selective toxicity of the DUSP1/6 inhibitor to CLL using the CLL-derived cell line MEC-1 compared to most other tested B cell and T cell lymphoma cell lines (Figure 2C).

To test whether the pharmacological inactivation of DUSP1/6 is a potential therapeutic option for CLL, we also determined its

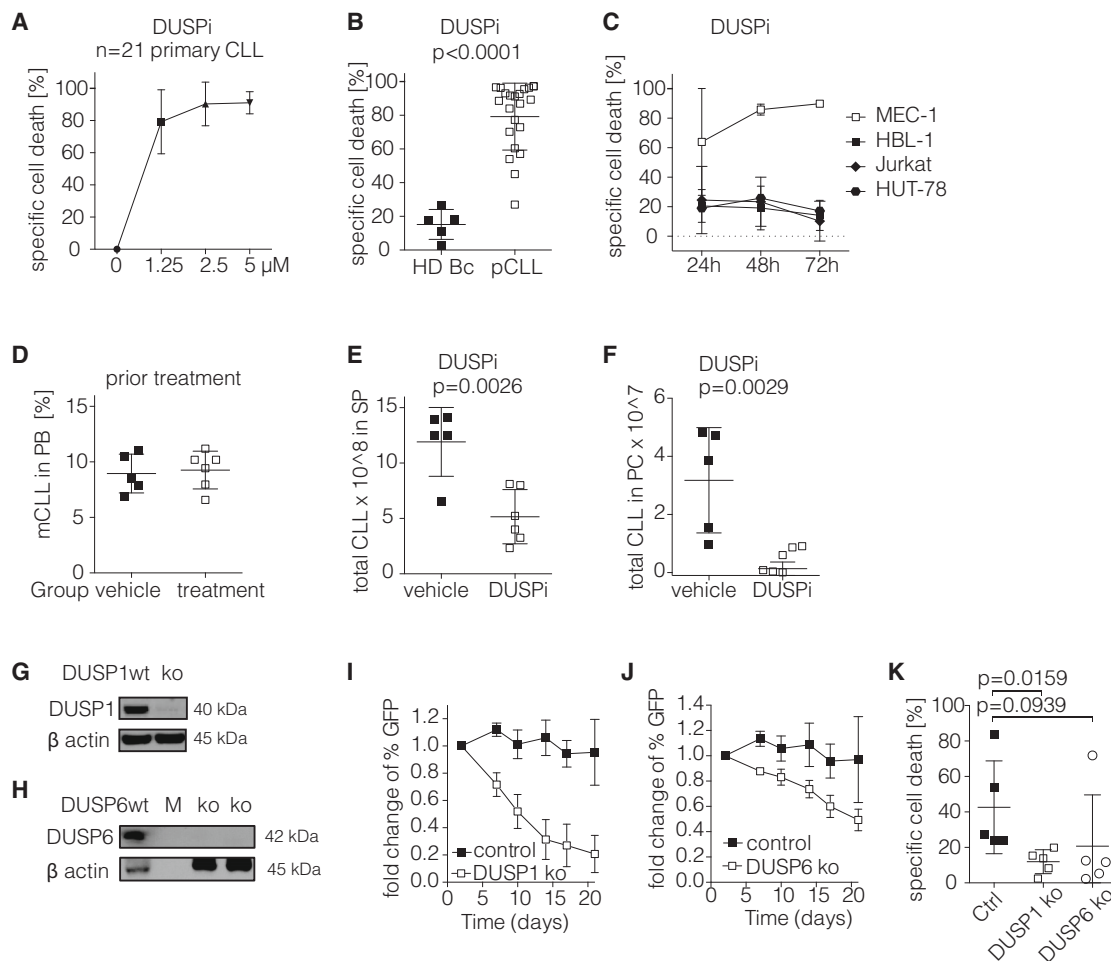


**Figure 2. DUSP1/6 inhibition is toxic specifically for CLL cells**

(A) Cytotoxic dose-response to increasing concentrations of the DUSP1/DUSP6 inhibitor BCI (0–5  $\mu$ M) in primary CLL samples (n = 21). Viability was determined after 48 h treatment by flow cytometry via DAPI staining. The percentage of specific cell death was calculated as follows:  $100 \times (\% \text{ dead cells} - \% \text{ baseline dead cells}) / (100\% - \% \text{ baseline dead cells})$ . Data are presented as mean values  $\pm$  SD.

(B) Specific cell death was calculated after viability measurement upon 48 h treatment with 1.25  $\mu$ M BCI *in vitro* in CD19<sup>+</sup> healthy donor-derived B cells (n = 5) compared to primary CLL cells (n = 21). Data are presented as mean values  $\pm$  SD. Statistical significance was assessed by a two-tailed unpaired Student's t test (p < 0.0001).

(C) Time course of *in vitro* treatment of CLL-derived cell line MEC-1 compared to human diffuse large B cell lymphoma cell line (HBL-1) and T cell lymphoma cell lines (Jurkat and HUT78). Specific cell death was determined after 24- to 72-h treatment with 5  $\mu$ M BCI (n = 2; independent experiments). Data are presented as mean values  $\pm$  SD.

(D–F) Analysis of *in vivo* treatment with the BCI derivative BCI-215. Splenocytes from TCL1-transgenic (tg) mice were transplanted in WT mice and treated with 10 mg/kg BCI-215 (n = 5) or vehicle control (5% DMSO in PBS) (n = 5) for 10 days. Content of CLL cells in peripheral blood (PB), spleen (SP), or peritoneal cavity (PC) in percent was determined by flow cytometry in vehicle control group and BCI-215 treatment group. Representative result for 2 independent experiments is shown. Data are presented as mean values  $\pm$  SD. (D) Evidence of CLL engraftment in non-irradiated C57Bl/6 WT mice prior treatment. (E) Content of total CLL counts ( $\times 10^8$ ) in spleen. Statistical significance was assessed by a two-tailed unpaired Student's t test (p = 0.0026). (F) Analysis of total CLL counts ( $\times 10^7$ ) in the PC. Statistical significance was assessed by a two-tailed unpaired Student's t test (p = 0.0029).

(G–K) Evaluation of genetic knockout experiments by CRISPR-Cas9 system in MEC-1 cell line. (G) Representative immunoblot of DUSP1 protein expression in MEC-1 WT cells compared to KO clone. Beta actin served as a loading control. (H) Immunoblot of DUSP6 expression in MEC-1 WT cells compared to KO clones. Loading: WT MEC1, M = marker, ko1, ko2 clone. Beta Actin served as a control. (I and J) *In vitro* competitor growth assays of successfully generated gene knockouts in MEC-1 cell line: (I) DUSP1 knockout clones (n = 2) and GFP<sup>+</sup> control clones (n = 2); (J) DUSP6 knockout clones (n = 2) and GFP<sup>+</sup> control clones (n = 2). Fold change of percent GFP was determined after mixing GFP<sup>+</sup> control cells and knockout cells. Data are presented as mean values (with  $\pm$ SD for knockout clones) of the fold change of GFP expression over time. (K) Specific cell death of WT control cell line versus DUSP1 and DUSP6 knockout clones was calculated after viability measurement by flow cytometry via DAPI staining after 48-h treatment with 1.25  $\mu$ M BCI or vehicle control. Pooled data from 4 independent experiments; data are presented as mean values  $\pm$  SD; statistical significance was assessed by a two-tailed unpaired Student's t test (DUSP1 p = 0.0939; DUSP6 p = 0.0159).

effect on CLL progression *in vivo*, using a TCL1-driven mouse model.<sup>31</sup> For *in vivo* treatments, we used a derivate of BCI (BCI-215) with reduced *in vivo* toxicity.<sup>32,33</sup> We injected CLL-bearing splenocytes from aged TCL1-tg mice into non-irradiated C57Bl/6 wild-type (WT) recipients and confirmed CLL engraftment prior to treatment initiation (Figure 2D). Then the mice were randomized to treatment or control groups and were treated with either BCI-215 (10 mg/kg) or vehicle daily for 10 consecutive days. This resulted in significantly reduced CLL content in the spleen and the peritoneal cavity, the major target organs for TCL1-derived murine CLL,<sup>31</sup> in the BCI-215 treated mice compared to the control mice (Figures 2E and 2F). Taken together, we showed that CLL cells are highly sensitive to DUSP1/6 inhibition, suggesting that negative regulation of the MAPK signaling pathway is important for their survival and disease progression *in vitro* and *in vivo*.

### Genetic disruption of DUSP1 or DUSP6 impairs CLL cell expansion

To exclude the possibility that the cytotoxic effects of BCI observed in CLL are primarily due to off-target effects by the small-molecule inhibitor, we next performed genetic knockout experiments to determine the role of DUSP1 and DUSP6 in CLL cell survival. To this end, we generated CRISPR-Cas9-mediated knockout lines of CLL-derived MEC-1 cells. Upon successful gene knockout of DUSP1 or DUSP6 in expanded single clones, as verified by western blotting (Figures 2G and 2H), we performed *in vitro* competitor growth assays to compare growth behaviors. For this, we mixed the expanded GFP-expressing clones, carrying either the DUSP1 or DUSP6 knockout or the Cas9 control vector (2 independent clones, respectively), with untransduced MEC-1 cells to visualize changes in their growth behavior under similar growth conditions. While the respective Cas9/GFP+ control cells were not affected (Figures 2I and 2J), both DUSP1 and DUSP6 knockout clones were outcompeted by WT MEC-1 cells, confirming the selective disadvantage of CLL cells lacking functional DUSP1 or DUSP6. Our attempts to generate DUSP1/DUSP6 double-knockout MEC-1 lines failed, suggesting that these are lethal (not shown). Notably, DUSP1 and DUSP6 knockout cells showed a markedly diminished response to the DUSP1/6 inhibitor, indicating that the observed specific apoptosis was largely attributed to on-target effects (Figure 2K). It should be noted that DUSP1 and DUSP6 knockout and Cas9+ control MEC-1 cells were expanded from single cells for several weeks prior to these experiments, which may limit the observed effects and the reproducibility of the effects upon acute DUSP1/6 inhibition. Nevertheless, these experiments confirm that the expression and activity of DUSP1 and DUSP6 are required for optimal CLL cell growth and survival.

### DUSP1/6 inhibition induces BCR/MAPK signaling in CLL cells followed by DNA damage response and apoptosis

To assess DUSP1/6-mediated signaling events in CLL, we used an unbiased screening approach and performed global phospho-proteome analysis of BCI- or vehicle-treated CLL cells. We first analyzed the early time points of BCI treatment for total phospho-proteomic alterations to validate the on-target effects of DUSP1/6 inhibition and to study the initial events using CLL

cells derived from a CLL patient (workflow depicted in Figure 3A). After 10 min of DUSP1/6 inhibitor treatment, we observed significant changes in the phosphorylation profile (Figures 3B, S2A, and S2B). Phospho-proteomic pathway analysis revealed that the phospho-sites of the BCR and MAPK networks were significantly deregulated (Figure 3C). As expected, we observed an increase in the phosphorylation of both ERK1 and ERK2 in DUSP1/6 inhibitor-treated CLL cells compared to control cells, confirming the on-target specificity of the inhibitor. To validate this finding in additional patients, we used western blotting to confirm the early phosphorylation of ERK1/2 upon treatment with the DUSP1/6 inhibitor in three additional primary CLL samples (Figure S2C).

To account for the potential heterogeneity among individual CLL patients in the downstream signaling responses induced by DUSP1/6 inhibition, we used the MEC-1 cell line as a model to study the downstream signaling events of DUSP1/6 inhibition in CLL. Here, we performed a time course experiment with subsequent phospho-proteome analysis using MEC-1 CLL cells, using later time points (0, 15, and 45 min) to gain insight into the molecular events associated with cell death. A heatmap with differentially phosphorylated proteins over all analyzed time points is shown, with four different clusters identified (Figures 4A and 4B). We then performed kinase prediction analysis to identify the kinases that mediate the observed downstream effects (Figure 4C). We identified the target sites of several kinases, including CDK1, PKC $\beta$ , and CK2 $\alpha$ . As expected, ERK1/2 target sites were significantly phosphorylated, confirming ERK1/2 activation upon DUSP1/6 inhibition. In addition, several of the predicted deregulated kinases are involved in DNA damage response (DDR), including CDK1,<sup>34,35</sup> CK2 $\alpha$ ,<sup>36</sup> and HIPK2.<sup>37</sup> Consistent with this, subsequent pathway analysis revealed that the DDR pathway is one of the most strongly regulated pathways upon DUSP1/6 inhibitor treatment in MEC-1 cells, with activating phosphorylation events on ATF2, c-JUN, and CHK1/2 kinases (Figure 4E).<sup>38,39</sup> We validated the activation of these pathways following DUSP1/6 inhibition in primary CLL samples (Figures S2D–S2G). In addition, we observed differential phosphorylation of molecules associated with the apoptotic pathway upon DUSP1/6 inhibition in our phospho-proteome screen, which is in line with the observed cell death upon DUSP1/6 inhibition in CLL (Figure 4F). Taken together, our phospho-proteome analysis suggests that DUSP1/6 inhibition induces MAPK signaling, followed by activation of the DDR and apoptotic pathways in CLL.

### Functional relevance of downstream signaling mediated by DUSP1/6 inhibition in CLL

Our phospho-proteome and western blot analyses revealed enhanced activation of the MAPK signaling pathway upon DUSP1/6 inhibition. To further validate this finding, we performed RNA sequencing analysis in MEC-1 and EHEB CLL cells with and without treatment with the DUSP1/6 inhibitor. We observed upregulation of genes associated with increased MAPK signaling (indicated by the KRAS signaling gene signature) as well as apoptosis-associated genes, corroborating our finding by phospho-proteomics (Figures 5A, 5B, S3A, and S3B). To test whether MAPK activation contributes to the cell

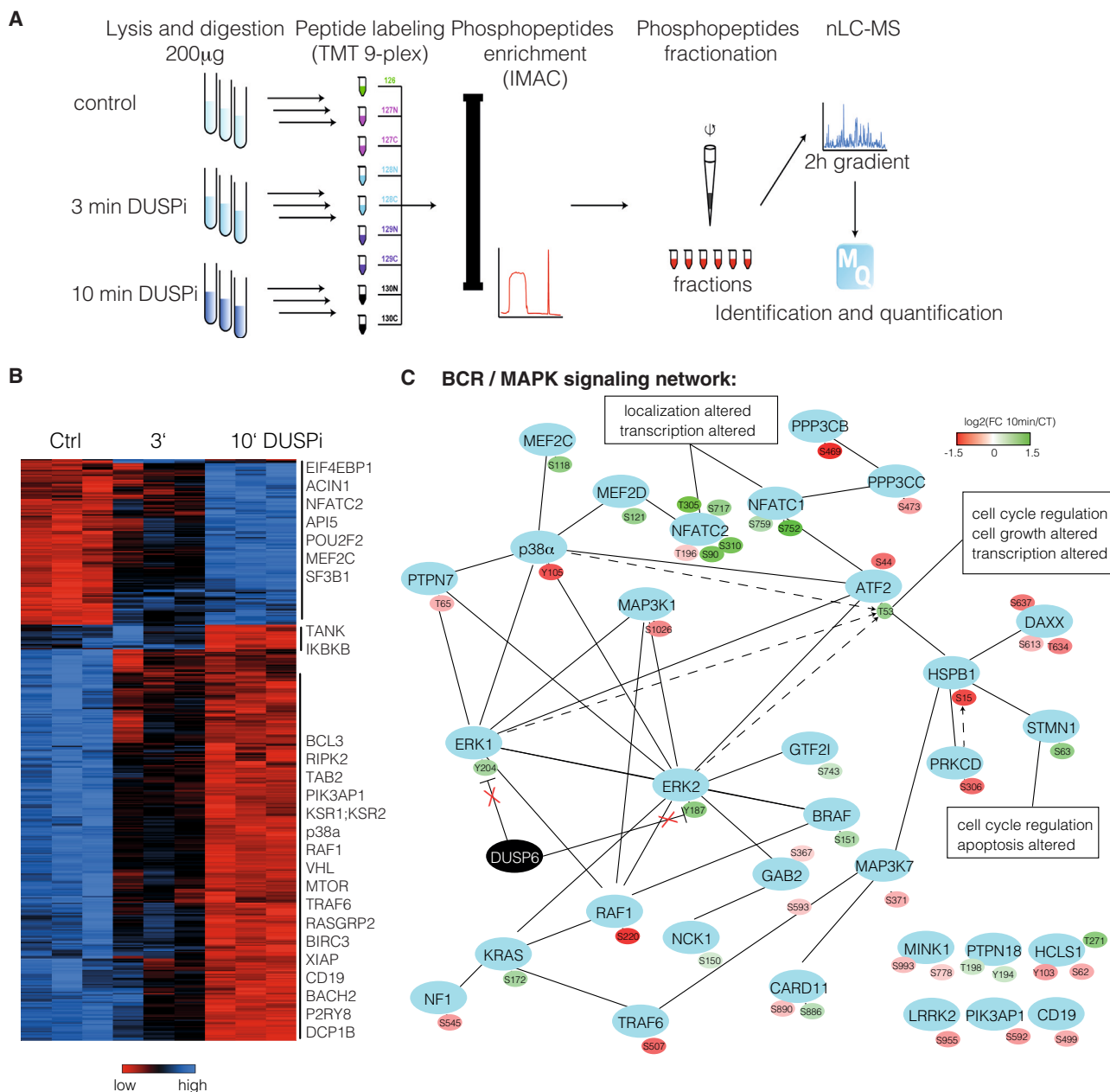


**Figure 3. DUSP1/6 inhibition induces MAPK signaling in CLL cells**

(A) Experimental setup of global phospho-proteome screen in primary CLL cells after DUSP1/DUSP6 inhibition (BCI; 2 µM).

(B) Heatmap of the phosphorylation profile of primary CLL cells treated for 3 or 10 min with the DUSP1/6 inhibitor BCI compared to untreated control (in 3 technical replicates) with a list of differentially phosphorylated proteins within the indicated clusters.

(C) Phospho-proteome analysis of primary CLL cells treated for 10 min with 2 µM BCI compared to untreated CLL cells. Map of regulated phospho-sites of BCR and MAPK network based on the KEGG pathway database.

death induced by DUSP1/6 inhibition in CLL functionally, we evaluated whether reducing ERK1/2 activation would mitigate the apoptotic effects of DUSP1/6 inhibition. Although MEK inhibition itself should be toxic to CLL cells,<sup>40</sup> we observed that co-treatment with the MEK inhibitor PD901 partially reversed the induction of specific cell death by the DUSP1/6 inhibitor in primary CLL cells (Figure 5C) and CLL cell lines (Figure S3C). We addi-

tionally validated these findings in primary CLL cells with the MEK inhibitors PD98059 (PD059) and trametinib (Tram) (Figures S3D and S3E). We also tested whether other members of the MAPK family, namely p38 and JNK, would contribute to DUSP1/6 inhibitor-mediated cell death. While JNK inhibition did not protect from BCI-mediated cytotoxicity, there was a trend for reduced cytotoxicity in p38-inhibitor-treated CLLs but

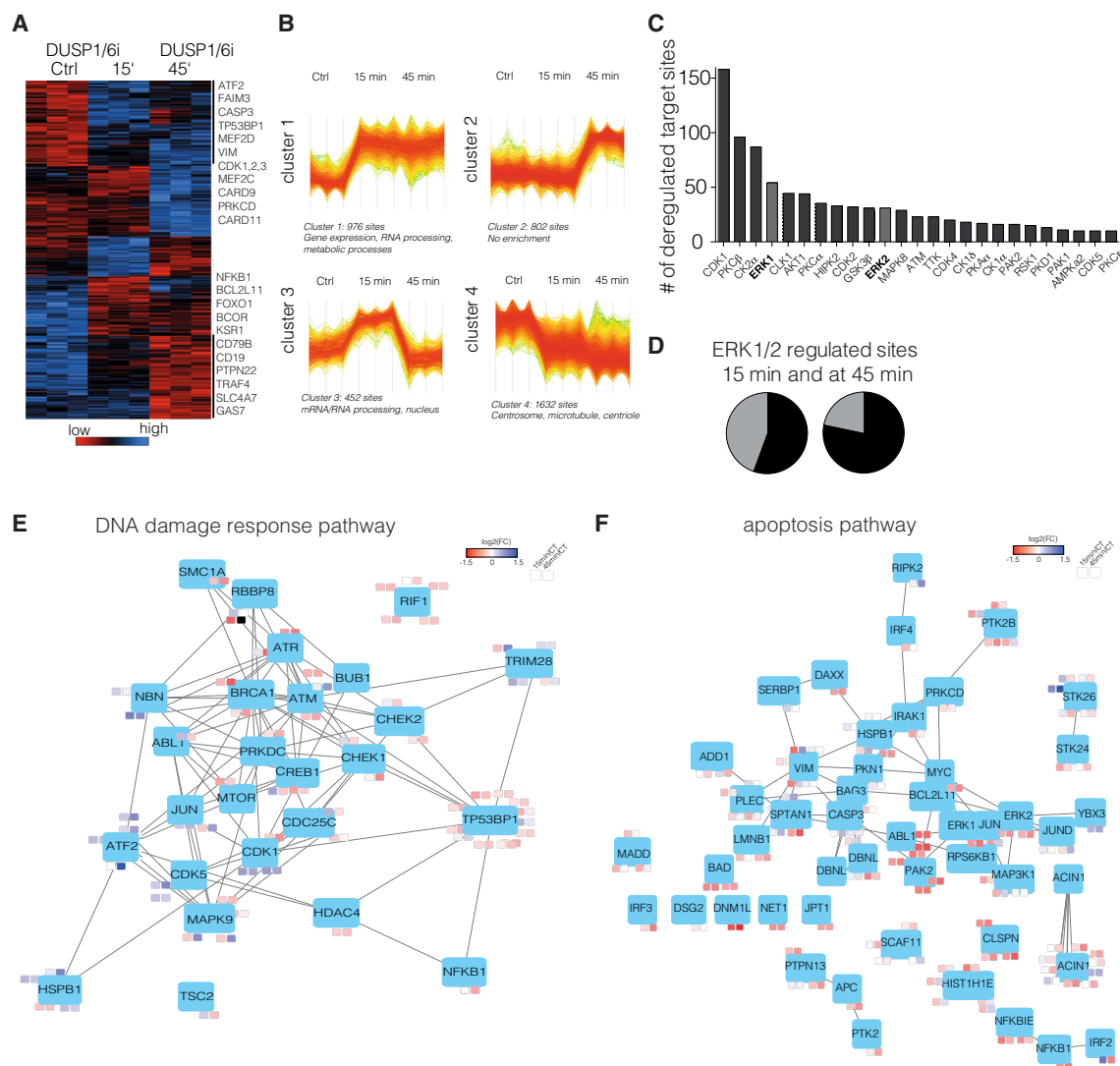


**Figure 4. Prolonged DUSP1/6 inhibition induces the activation of DNA damage response and apoptosis in CLL**

(A) Heatmap of the phosphorylation profile of MEC-1 cells treated for 15 or 45 min with the DUSP1/6 inhibitor (BCI; 5  $\mu$ M) compared to untreated control MEC-1 cells (in 3 technical replicates) with a list of differentially phosphorylated proteins within the indicated region.

(B) Unsupervised hierarchical cluster analysis revealed 4 clusters of differentially regulated phospho-sites; cluster 1: up at 15- and 45-min treatment; cluster 2: up only at 45-min treatment; cluster 3: up only at 15-min treatment; cluster 4: down at 15- and 45-min treatment; Gene Ontology analysis was performed for enrichment of target proteins in specific pathways and is listed below the individual clusters.

(C) Prediction of upstream kinases responsible for the observed differentially regulated phosphorylation sites after 15-min DUSP1/6 inhibition using the NetworkKIN algorithm.

(D) Pie chart of ERK1/2 up- and downregulated target sites upon DUSP1/6 inhibition for 15 and 45 min.

(E and F) Phospho-proteome analysis of MEC-1 treated for 15 and 45 min with DUSP1/6 inhibitor (BCI; 5  $\mu$ M) compared to untreated MEC-1 cells using ANOVA analysis. DNA damage network (E) and apoptosis network (F) were identified as differentially regulated using Cytoscape and the PhosphoPath plugin.

did not reach statistical significance (Figures S3F and S3G). Based on the activation of the DDR pathway observed in our phospho-proteome screen, we investigated whether DUSP1/6 inhibition promotes DNA damage in CLL cells. To this end, we analyzed the phosphorylation of  $\gamma$ H2AX, one of the earliest cellular responses to DNA double-strand breaks, using flow cytometry. Indeed, phospho- $\gamma$ H2AX levels increased upon DUSP1/6 inhibitor treatment compared to the control patient-derived CLL cells in a dose-dependent manner (Figure 5D), while

isotype control-stained cells did not show increased fluorescence (Figure S3H). Similar results were obtained using western blotting (Figure S3I). It should be noted that  $\gamma$ H2AX phosphorylation occurs only after 4 h of DUSP1/6 inhibitor treatment and was therefore not detected in our global phospho-proteome analysis, where we used early time points to avoid secondary effects on high levels of cell death (Figures S3J and S3K). To analyze whether the DDR was a consequence of increased MAPK signaling induced by DUSP1/6 inhibition, we measured

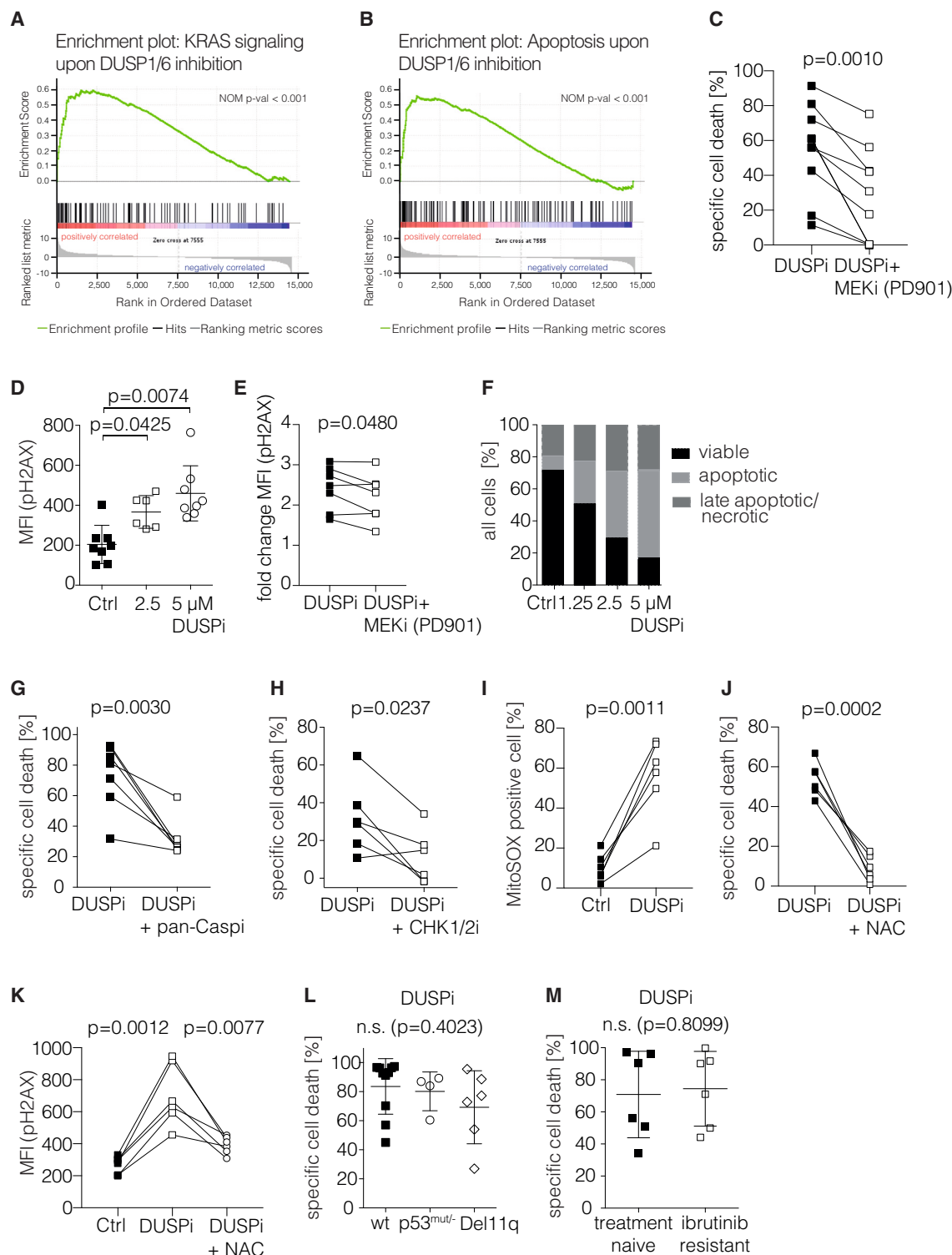


**Figure 5. Functional relevance of the activation of ERK and DNA damage response for DUSP1/6 inhibition-mediated apoptosis**

(A and B) Gene set enrichment analysis (GSEA) results for the association with (A) “KRAS signaling” and (B) “apoptosis” of the CLL cell line MEC-1 after DUSP1/6 inhibition with BCI (2.5  $\mu$ M) for 4 h. (A) Enrichment Score (ES) = 0.59481156; normalized enrichment score (NES) = 2.09; nominal p value < 0.001; false discovery rate (FDR) q value < 0.001; family-wise error rate (FWER) p value < 0.001.

(B) ES = 0.5562553; NES = 2.09; nominal p value < 0.001; FDR q value = 0.000125; FWER p value = 0.001.

(legend continued on next page)

the phosphorylation of  $\gamma$ H2AX with and without pretreatment with the MEK inhibitors PD901 and PD059 in patient-derived CLL cells. We observed that both inhibitor treatments significantly reduced the DUSP1/6-mediated upregulation of phospho- $\gamma$ H2AX in multiple independent experiments (Figures 5E and S3L). Although MEK inhibition only partially reverted the effects, our data clearly show that ERK activation contributes to DUSP1/6-mediated cell death at least partially via activation of DDR.

In addition, we analyzed whether DUSP1/6 inhibition induces classical apoptosis in CLL, as indicated by phospho-proteome analysis. Annexin V staining of primary human CLL cells treated with DUSP1/6 inhibitor revealed strong exposure of phosphatidylserine on the outer membrane (Figure 5F). Consistent with this, co-treatment with the pan-caspase inhibitor QVD (or Emricasan) significantly reduced the toxic effect of DUSP1/6 inhibition alone (Figures 5G and S4A). Absolute CLL cell viability increased upon caspase inhibition by reducing spontaneous apoptosis in cultured CLL cells (Figure S4B). As DDR can either protect cells from apoptosis or promote the induction of cell death, we next investigated whether the observed activation of the DDR pathway promoted the cytotoxic effects of DUSP1/6 inhibition in CLL cells. To do this, we investigated whether inhibition of CHK1/2 kinases, critical effectors of the DDR pathway (which were also differentially phosphorylated in our MEC-1 phospho-proteome screen), reduced the cytotoxic effects of DUSP1/6 inhibition. While CHK1/2 inhibition alone was not toxic to the CLL cells at the tested concentrations (Figure S4C), concomitant treatment of CLL with DUSP1/6 and CHK1/2 inhibitors ameliorated the toxic effect of DUSP1/6 inhibition alone (Figure 5H). Similar effects were observed using a CHK1-specific inhibitor (Figure S4D). Nevertheless, ATM inhibition did not significantly alter the effects of DUSP1/6 inhibition on CLL cell

survival, indicating that this pathway is less important in the downstream response (Figure S4E). Therefore, CHK- but not ATM-mediated signaling contributes to the apoptotic effect of DUSP inhibition in CLL.

The MAPK/ERK signaling pathway has been reported to play various roles in regulating mitochondrial homeostasis, activity, and structure.<sup>41–44</sup> Reactive oxygen species (ROS) are a by-product of mitochondrial activity. Altered mitochondrial function or structure could result in increased ROS production upon ERK activation. Due to their reactive nature, ROS can induce DNA damage. We therefore tested whether mitochondrial ROS levels were altered upon DUSP inhibition in CLL, which could ultimately lead to DNA damage.<sup>45</sup> Using a fluorescent indicator of mitochondrial superoxide, we observed that DUSP inhibition strongly upregulated mitochondrial ROS levels in CLL (Figure 5I). Importantly, blocking ROS levels by N-acetylcysteine (NAC) strongly reduced the cytotoxic effect of DUSP inhibition, confirming a direct relevance of ROS for DUSP inhibitor-mediated cell death induction (Figure 5J). Furthermore, we observed that NAC treatment also reduced the DUSP inhibitor-induced phosphorylation of  $\gamma$ H2AX, indicating that ROS is at least partially responsible for the observed DNA damage upon DUSP inhibition in CLL (Figure 5K).

Taken together, our analysis confirmed the functional relevance of the DDR pathway in apoptosis induction in CLL cells upon DUSP1/6 inhibition, which is at least partially mediated by mitochondrial ROS and the activation of CHK1/2.

### DUSP1/6 inhibition is effective in drug-resistant CLL

Importantly, p53, a major effector in the induction of apoptosis as a consequence of DNA damage, seems to be dispensable for mediating DUSP1/6 inhibition-promoted cell death, as the MEC-1 CLL cell line, which carries both 17p deletion (Del17p)

(C) Specific cell death was calculated after flow cytometric viability analysis by DAPI staining. Primary CLL cells were pre-treated for 1 h with 5  $\mu$ M MEK inhibitor (PD901) followed by DUSP1/6 inhibitor treatment (BCI; 1.25  $\mu$ M) or control treatment for 48 h ( $n = 10$ , pooled data from 3 independent experiments). Statistical significance was assessed by a two-tailed paired Student's  $t$  test ( $p = 0.0010$ ).

(D) Analysis of the phosphorylation of  $\gamma$ H2AX mean fluorescence intensity (MFI) of primary CLL cells treated with BCI (2.5  $\mu$ M and 5  $\mu$ M) for 24 h. MFI values  $\pm$  SD. Statistical significance was assessed by a two-tailed paired Student's  $t$  test (2.5  $\mu$ M  $p = 0.0425$ ; 5  $\mu$ M  $p = 0.0074$ ).

(E) Analysis of the fold change of the phosphorylation of the  $\gamma$ H2AX mean fluorescence intensity (MFI) of primary CLL cells pre-treated for 1 h with 5  $\mu$ M MEK inhibitor (PD901) followed by DUSP1/6 inhibitor treatment (BCI; 2.5  $\mu$ M) or control treatment for 24 h. Statistical significance was assessed by a two-tailed paired Student's  $t$  test,  $p = 0.0480$  ( $n = 7$ , pooled data from 2 independent experiments).

(F) Flow cytometric analysis of annexin V staining of primary CLL cells treated with DUSP1/6 inhibitor (BCI; 0–5  $\mu$ M) for 24 h. Classification of the cells in necrotic, late apoptotic, apoptotic, and viable cell stages specified as percent of all cells; representative example for  $n = 4$  primary CLL cases.

(G and H) Specific cell death was calculated after flow cytometric viability analysis by DAPI staining. Primary CLL cells were pre-treated for 1 h with (G) 5  $\mu$ M of the pan-caspase inhibitor QVD or (H) 50 nM of the CHK1/2 kinase inhibition AZD6672 followed by DUSP1/6 inhibitor treatment (BCI; 1  $\mu$ M) or control treatment for 48 h. Statistical significance was assessed by a two-tailed paired Student's  $t$  test.

(G)  $p = 0.0030$ ;  $n = 7$ . (H)  $p = 0.0237$ ;  $n = 6$ .

(I) Flow cytometry analysis of MitoSOX-positive primary CLL cells treated with BCI (1.25  $\mu$ M) or control treatment for 24 h. Statistical significance was assessed by a two-tailed paired Student's  $t$  test,  $p = 0.0011$  ( $n = 6$ , pooled data from 2 independent experiments).

(J) Specific cell death was calculated after flow cytometric viability analysis by DAPI staining. Primary CLL cells were pre-treated for 1 h with 50  $\mu$ M N-acetylcysteine (NAC) followed by DUSP1/6 inhibitor treatment (BCI; 1.25  $\mu$ M) or control treatment for 24 h ( $n = 6$ , pooled data from 2 independent experiments). Statistical significance was assessed by a two-tailed paired Student's  $t$  test ( $p = 0.0002$ ).

(K) Analysis of the phosphorylation of  $\gamma$ H2AX MFI of primary CLL cells pre-treated for 1 h with 50  $\mu$ M NAC followed by DUSP1/6 inhibitor treatment (BCI; 2.5  $\mu$ M) or control treatment for 24 h. Statistical significance was assessed by a two-tailed paired Student's  $t$  test,  $p = 0.0012$ ,  $p = 0.0077$  ( $n = 6$ , pooled data from 2 independent experiments).

(L) Response of primary CLL cells with Del11q or Del17p/p53 mutation toward DUSP1/6 inhibitor (BCI; 1.25  $\mu$ M) compared to patients without these alterations. Data represented as specific cell death (%) after DAPI measurement by flow cytometry. Data are presented as mean values  $\pm$  SD. Statistical significance was assessed by a two-tailed unpaired Student's  $t$  test (n.s.  $p = 0.2803$ ).

(M) Specific cell death of treatment-naïve ( $n = 6$ ) and ibrutinib-resistant ( $n = 6$ ) primary CLL samples after 48 h BCI treatment (1  $\mu$ M). Data are presented as mean values  $\pm$  SD. Statistical significance was assessed by a two-tailed unpaired Student's  $t$  test (n.s.  $p = 0.8099$ ).

and TP53 mutations, is sensitive to DUSP1/6 inhibition (shown in Figure 2C). Similar to the MEC-1 cell line, primary CLL cells frequently harbor genetic alterations in the DDR pathway. Up to 8% of chemotherapy-naïve patients carry Del17p, and up to 80% of these carry mutations in TP53 on the second allele.<sup>46,47</sup> This loss of functional p53 is associated with resistance to chemotherapeutic agents. In addition, ATM is frequently inactivated in CLL and is associated with reduced apoptosis induction in response to chemotherapeutic agents.<sup>48</sup> To determine whether genetic alterations in the DDR pathway affect the response rate to DUSP1/6 inhibition in CLL, we compared the cytotoxic response toward DUSP1/6 inhibition in CLL samples carrying p53 mutations or Del17p or Del11q, leading to a loss of functional p53 or ATM, respectively, compared to WT p53- or ATM-expressing cases. Although there was a minor reduction in the mean cell death induction, there was no significant difference in the cytotoxic response to DUSP1/6 inhibition between cases with and without functional p53/ATM (Figure 5L). Although this analysis is based on a limited number of samples with the respective genetic alterations, it indicates that DUSP1/6 inhibition remains highly effective in killing CLL cells carrying mutations that disrupt a functional ATM/p53-mediated DDR.

Based on the clinical need to identify novel treatment options for clinically ibrutinib-refractory CLL, we compared the effects of DUSP1/6 inhibition on primary CLL in treatment-naïve patients with ibrutinib-refractory cases. Here, we found that ibrutinib-resistant CLL cells remained sensitive to BCI treatment with similar induction of specific cell death compared to treatment-naïve CLL cells analyzed in parallel (Figure 5M). Taken together, we showed that DUSP1/6 inhibition is highly effective in inducing cytotoxicity in all tested CLL subsets and may be particularly useful for treating treatment-resistant and refractory CLL.

## DISCUSSION

In this study, we discovered a previously unknown role for DUSP1 and DUSP6 in limiting MAPK signaling in CLL, thereby preventing apoptosis. We discovered that high mRNA expression of the negative regulator DUSP6 is linked to a poor clinical outcome in CLL. Both DUSP1 and DUSP6 expressions are necessary for maintaining optimal CLL cell proliferation. Inhibition of DUSP1 and DUSP6 phosphatase activities limits CLL cell survival *in vitro* and disease development *in vivo*. Mechanistically, we discovered that inhibiting DUSP1/6 triggers activation of the BCR/MAPK signaling pathway, causing DNA damage-mediated apoptosis. This pro-apoptotic effect of DUSP1/6 inhibition was strong in drug-resistant CLL. Therefore, we identified the MAPK-negative regulators DUSP1 and DUSP6 as novel treatment targets, particularly for drug-resistant CLL.

By acting as negative regulators of the MAPK signaling pathway, dual-specific phosphatases can restrict tumor growth and promote carcinogenesis and drug resistance.<sup>49</sup> Understanding the downstream processes of DUSP1/6 inhibition should aid in determining malignancies that are responsive to the drug. We used an unbiased phospho-proteome screen to determine the cause of cell death in response to DUSP1/6 inhibition in CLL. ERK1/2 activation was found to be important for inducing CLL apoptosis upon DUSP1/6 inhibition, which may

appear surprising as ERK1/2 activity is most commonly associated with cell proliferation and survival. However, active ERK1/2 has also been linked to cell death during negative selection of B cells to prevent autoimmunity.<sup>16</sup> We hypothesized that CLL-specific checkpoints that limit B cell growth stem from the inherent sensitivity of B cells to strong BCR/MAPK signaling that mimics autoimmunity, resulting in the indolent nature of the disease. Consequently, CLL cells die rather than proliferate rapidly when MAPK signaling is induced to non-physiological levels. In contrast to DUSP6, DUSP1 mRNA levels do not correlate with disease progression, which could be due to the regulation of DUSP1 at the post-transcriptional level.<sup>50</sup>

We observed high levels of mitochondrial ROS upon DUSP inhibition in CLL. While low levels of ROS can serve as signaling molecules, excessive ROS production can lead to oxidative stress, which can damage cellular components, including DNA. This includes the formation of 8-oxoguanine (8-oxoG) lesions, DNA strand breaks, and DNA-protein cross-links.<sup>45</sup> Mitochondrial ROS can disrupt the balance of pro-survival and pro-apoptotic factors, leading to mitochondrial membrane permeabilization, release of cytochrome c, and activation of caspases, ultimately resulting in cell death.<sup>51</sup>

Drug resistance is a major obstacle to the treatment of CLL. Despite high initial response rates, a considerable percentage of patients receiving chemotherapy or targeted therapies experience relapse with progressive and refractory disease. Drug resistance has been linked to the mutation of specific drug-binding sites or the activation of alternative pro-survival pathways, including the MAPK signaling pathway.<sup>9–11</sup> In addition, particular genetic abnormalities are associated with drug resistance to chemotherapeutic treatments, such as the deletion of ATM or p53, which are important molecules in DNA damage-mediated apoptosis.<sup>46,48</sup> Although we observed that the DDR was also involved in DUSP1/6 inhibitor-mediated cytotoxicity, DUSP1/6 suppression efficiently killed p53-mutated and ATM-deleted CLL, suggesting that alternative pathways that can induce mitochondrial ROS followed by DDR-mediated cell death, such as CHK1 and/or ATR activation, remain intact.<sup>52</sup>

Activation of ERK1/2, JNK, and p38 determines the sensitivity to therapy in a variety of cancers, including CLL,<sup>53,54</sup> and resistance emerging from patients treated with the PI3K inhibitor idelalisib results in elevated MAPK signaling to counteract PI3K pathway inhibition.<sup>55</sup> Based on our findings, we hypothesize that cells with high levels of ERK signaling would be equally vulnerable to DUSP1/6 inhibition, rendering DUSP1/6 inhibition an interesting approach for drug-resistant CLL. Negative regulation of MAPK via DUSP1 (via JNK suppression) also promotes drug resistance in cancer entities,<sup>56</sup> including osteosarcoma,<sup>57</sup> lung cancer cells,<sup>58</sup> and ovarian cancer.<sup>59</sup> This JNK regulation may contribute to the toxicity induced in CLL by DUSP1/6 inhibition. In clinical patient care, limited responses against the BTK inhibitor ibrutinib are highly relevant; therefore, we investigated whether DUSP1/6 inhibition is also effective against ibrutinib-refractory cases. Based on our findings, these refractory CLL cells are equally vulnerable to DUSP1/6 inhibition in treatment-naïve patients. Therefore, DUSP1/6 inhibition may be equally effective in treating drug-resistant CLL.

Taken together, our findings reveal that in CLL, negative control of MAPK signaling is required to avoid DNA damage response-mediated cell death. We show that high DUSP6 expression is associated with poor clinical outcomes in CLL and may indicate high MAPK signaling, for example, induced by activating mutations of NRAS or BRAF. Furthermore, we demonstrated that inhibiting the activity of DUSP1/6 phosphatases causes DNA damage and cell death in CLL, and that treatment-resistant CLL cases remain sensitive to DUSP1/6 inhibition. As a result, we propose intermittent DUSP1/6 inhibition as a novel approach for CLL therapy, either in combination with kinase inhibition, to potentially boost the efficacy of both solo treatments, or to treat kinase inhibitor-resistant disease.

### Limitations of the study

One significant limitation in our study is the use of a dual-specific inhibitor that simultaneously targets DUSP1 and DUSP6 in the majority of experiments, which hinders our ability to distinguish the individual effects of inhibiting each molecule. Since genetic alteration of primary CLL cells is technically very challenging, we used the CLL-derived cell line MEC-1 for CRISPR-mediated deletion of either DUSP1 or DUSP6. This line is EBV-positive and grows *in vitro* without support of the microenvironment and therefore lacks critical characteristics of primary CLL. In addition, to generate the knockout, single clones expand for weeks before subsequent analysis can be performed, enabling multiple adaptation processes to occur. Therefore, the genetic knockout experiments have limited value when comparing it to the effects to acute DUSP inhibition. An additional limitation of our study is the limited insight into potential effects of DUSP inhibition *in vivo* on the host immune system.

### STAR★METHODS

Detailed methods are provided in the online version of this paper and include the following:

- KEY RESOURCES TABLE
- RESOURCE AVAILABILITY
  - Lead contact
  - Materials availability
  - Data and code availability
- EXPERIMENTAL MODEL AND SUBJECT DETAILS
  - Mice
  - Cell lines and primary CLL cells
- METHOD DETAILS
  - Inhibitor treatment and subsequent analysis
  - Generating DUSP1 and DUSP6 knock outs
  - Oligo annealing and phosphorylation
  - Golden gate cloning
  - Plasmid safe ligation
  - Nucleofection-based transient transfection
  - Retroviral CRISPR knockout generation
  - Pipetting scheme
  - Programm
  - Immunoblot
  - Competition assay
  - AnnexinV staining

- Phospho-proteome screen
- TMT labeling
- Phospho-peptide enrichment and fractionation
- LC-MS/MS analysis
- Data processing
- Data analysis for phospho-proteome data
- RNA preparations and RNA sequencing
- QUANTIFICATION AND STATISTICAL ANALYSIS

### SUPPLEMENTAL INFORMATION

Supplemental information can be found online at <https://doi.org/10.1016/j.celrep.2023.113017>.

### ACKNOWLEDGMENTS

We would like to thank Tanja Neumeier and Nicole Beck for excellent technical support. This work was funded by the German Cancer Aid (Deutsche Krebshilfe, Max Eder Grant to M.B., Project ID 70114720), German Research Foundation (Deutsche Forschungsgemeinschaft, DFG) – Project ID 360372040 – SFB 1335/P02 awarded to M.B., P01 to J.R., and Wilhelm Sander Foundation (Project ID 2018.111.1 to M.B.).

### AUTHOR CONTRIBUTIONS

V.E., L.B., M.S., P.G., A.V.M., L.P., and M.H.A.M.F. designed and performed research. B.K., I.R., M.M., J.J., and J.R. designed the research. J.L., R.R., and T.E. analyzed the data. S.H., T.Z., and C.-M.W. contributed CLL samples. M.B. designed and performed the research and wrote the paper.

### DECLARATION OF INTERESTS

S.H. is an employee of and holds equity interest in Roche/Genentech. S.H. has received research funding from Bristol Myers-Squibb and Novartis. S.H. has been a consultant for Bristol Myers-Squibb, Novartis, Merck, Abbvie, and Roche.

### INCLUSION AND DIVERSITY

One or more of the authors of this paper self-identifies as an underrepresented ethnic minority in their field of research or within their geographical location. One or more of the authors of this paper self-identifies as a gender minority in their field of research. One or more of the authors of this paper self-identifies as a member of the LGBTQIA+ community.

Received: March 13, 2023

Revised: June 8, 2023

Accepted: August 6, 2023

Published: October 4, 2023

### REFERENCES

1. Dühren-von Minden, M., Übelhart, R., Schneider, D., Wossning, T., Bach, M.P., Buchner, M., Hofmann, D., Surova, E., Follo, M., Köhler, F., et al. (2012). Chronic lymphocytic leukaemia is driven by antigen-independent cell-autonomous signalling. *Nature* 489, 309–312. <https://doi.org/10.1038/nature11309>.
2. Hamblin, T.J., Davis, Z., Gardiner, A., Oscier, D.G., and Stevenson, F.K. (1999). Unmutated Ig V(H) genes are associated with a more aggressive form of chronic lymphocytic leukemia. *Blood* 94, 1848–1854.
3. Maurer, K., Zahrieh, D., Gorgun, G., Li, A., Zhou, J., Ansén, S., Rassenti, L.Z., and Gribben, J.G. (2005). Immunoglobulin gene segment usage, location and immunogenicity in mutated and unmutated chronic lymphocytic leukaemia. *Br. J. Haematol.* 129, 499–510. <https://doi.org/10.1111/j.1365-2141.2005.05480.x>.

4. Messmer, B.T., Albesiano, E., Efremov, D.G., Ghiotto, F., Allen, S.L., Koltz, J., Foa, R., Damle, R.N., Fais, F., Messmer, D., et al. (2004). Multiple distinct sets of stereotyped antigen receptors indicate a role for antigen in promoting chronic lymphocytic leukemia. *J. Exp. Med.* 200, 519–525. <https://doi.org/10.1084/jem.20040544>.
5. Kittai, A.S., and Woyach, J.A. (2019). Resistance Mechanisms to Targeted Agents in Chronic Lymphocytic Leukemia. *Cancer J.* 25, 428–435. <https://doi.org/10.1097/PPO.0000000000000406>.
6. Landau, D.A., Tausch, E., Taylor-Weiner, A.N., Stewart, C., Reiter, J.G., Bahlo, J., Kluth, S., Bozic, I., Lawrence, M., Böttcher, S., et al. (2015). Mutations driving CLL and their evolution in progression and relapse. *Nature* 526, 525–530. <https://doi.org/10.1038/nature15395>.
7. Giménez, N., Martínez-Trillos, A., Montraveta, A., Lopez-Guerra, M., Rosich, L., Nadeu, F., Valero, J.G., Aymerich, M., Magnano, L., Rozman, M., et al. (2019). Mutations in the RAS-BRAF-MAPK-ERK pathway define a specific subgroup of patients with adverse clinical features and provide new therapeutic options in chronic lymphocytic leukemia. *Haematologica* 104, 576–586. <https://doi.org/10.3324/haematol.2018.196931>.
8. Vendramini, E., Bomben, R., Pozzo, F., Benedetti, D., Bittolo, T., Rossi, F.M., Dal Bo, M., Rabe, K.G., Pozzato, G., Zaja, F., et al. (2019). KRAS, NRAS, and BRAF mutations are highly enriched in trisomy 12 chronic lymphocytic leukemia and are associated with shorter treatment-free survival. *Leukemia* 33, 2111–2115. <https://doi.org/10.1038/s41375-019-0444-6>.
9. Herling, C.D., Abedpour, N., Weiss, J., Schmitt, A., Jachimowicz, R.D., Merkel, O., Cartolano, M., Oberbeck, S., Mayer, P., Berg, V., et al. (2018). Clonal dynamics towards the development of venetoclax resistance in chronic lymphocytic leukemia. *Nat. Commun.* 9, 727. <https://doi.org/10.1038/s41467-018-03170-7>.
10. Pandzic, T., Larsson, J., He, L., Kundu, S., Ban, K., Akhtar-Ali, M., Hellström, A.R., Schuh, A., Clifford, R., Blakemore, S.J., et al. (2016). Transposon Mutagenesis Reveals Fludarabine Resistance Mechanisms in Chronic Lymphocytic Leukemia. *Clin. Cancer Res.* 22, 6217–6227. <https://doi.org/10.1158/1078-0432.CCR-15-2903>.
11. Takahashi, K., Hu, B., Wang, F., Yan, Y., Kim, E., Vitale, C., Patel, K.P., Strati, P., Gumbs, C., Little, L., et al. (2018). Clinical implications of cancer gene mutations in patients with chronic lymphocytic leukemia treated with lenalidomide. *Blood* 131, 1820–1832. <https://doi.org/10.1182/blood-2017-11-817296>.
12. Chen, Y., Germano, S., Shelmani, G., Kluczna, D., Jayne, S., Dyer, M.J.S., and Macip, S. (2018). Paradoxical activation of alternative pro-survival pathways determines resistance to MEK inhibitors in chronic lymphocytic leukaemia. *Br. J. Haematol.* 182, 921–924. <https://doi.org/10.1111/bjh.14880>.
13. Wagner, E.F., and Nebreda, A.R. (2009). Signal integration by JNK and p38 MAPK pathways in cancer development. *Nat. Rev. Cancer* 9, 537–549. <https://doi.org/10.1038/nrc2694>.
14. Cagnol, S., and Chambard, J.C. (2010). ERK and cell death: mechanisms of ERK-induced cell death—apoptosis, autophagy and senescence. *FEBS J.* 277, 2–21. <https://doi.org/10.1111/j.1742-4658.2009.07366.x>.
15. Hollmann, C.A., Owens, T., Nalbantoglu, J., Hudson, T.J., and Sladek, R. (2006). Constitutive activation of extracellular signal-regulated kinase predisposes diffuse large B-cell lymphoma cell lines to CD40-mediated cell death. *Cancer Res.* 66, 3550–3557. <https://doi.org/10.1158/0008-5472.CAN-05-2498>.
16. Limnander, A., Depeille, P., Freedman, T.S., Liou, J., Leitges, M., Kurosaki, T., Roose, J.P., and Weiss, A. (2011). STIM1, PKC- $\delta$  and RasGRP set a threshold for proapoptotic Erk signaling during B cell development. *Nat. Immunol.* 12, 425–433. <https://doi.org/10.1038/ni.2016>.
17. Seger, R., and Krebs, E.G. (1995). The MAPK signaling cascade. *Faseb. J.* 9, 726–735.
18. Zhang, Z., Kobayashi, S., Borczuk, A.C., Leidner, R.S., Laframboise, T., Levine, A.D., and Halmos, B. (2010). Dual specificity phosphatase 6 (DUSP6) is an ETS-regulated negative feedback mediator of oncogenic ERK signaling in lung cancer cells. *Carcinogenesis* 31, 577–586. <https://doi.org/10.1093/carcin/bgq020>.
19. Furukawa, T., Sunamura, M., Motoi, F., Matsuno, S., and Horii, A. (2003). Potential tumor suppressive pathway involving DUSP6/MKP-3 in pancreatic cancer. *Am. J. Pathol.* 162, 1807–1815. [https://doi.org/10.1016/S0002-9440\(10\)64315-5](https://doi.org/10.1016/S0002-9440(10)64315-5).
20. Ramkissoon, A., Chaney, K.E., Milewski, D., Williams, K.B., Williams, R.L., Choi, K., Miller, A., Kalin, T.V., Pressey, J.G., Szabo, S., et al. (2019). Targeted Inhibition of the Dual Specificity Phosphatases DUSP1 and DUSP6 Suppress MPNST Growth via JNK. *Clin. Cancer Res.* 25, 4117–4127. <https://doi.org/10.1158/1078-0432.CCR-18-3224>.
21. Shojaei, S., Caeser, R., Buchner, M., Park, E., Swaminathan, S., Hurtz, C., Geng, H., Chan, L.N., Klemm, L., Hofmann, W.K., et al. (2015). Erk Negative Feedback Control Enables Pre-B Cell Transformation and Represents a Therapeutic Target in Acute Lymphoblastic Leukemia. *Cancer Cell* 28, 114–128. <https://doi.org/10.1016/j.ccell.2015.05.008>.
22. Lu, J., Cannizzaro, E., Meier-Abt, F., Scheinost, S., Bruch, P.M., Giles, H.A., Lütge, A., Hülle, J., Wagner, L., Giacomelli, B., et al. (2021). Multi-omics reveals clinically relevant proliferative drive associated with mTOR-MYC-OXPHOS activity in chronic lymphocytic leukemia. *Nat. Can.* 2, 853–864. <https://doi.org/10.1038/s43018-021-00216-6>.
23. Dietrich, S., Oleś, M., Lu, J., Sellner, L., Anders, S., Velten, B., Wu, B., Hülle, J., da Silva Liberio, M., Walther, T., et al. (2018). Drug-perturbation-based stratification of blood cancer. *J. Clin. Invest.* 128, 427–445. <https://doi.org/10.1172/JCI93801>.
24. Herishanu, Y., Pérez-Galán, P., Liu, D., Biancotto, A., Pittaluga, S., Vire, B., Gibellini, F., Njuguna, N., Lee, E., Stennett, L., et al. (2011). The lymph node microenvironment promotes B-cell receptor signaling, NF- $\kappa$ B activation, and tumor proliferation in chronic lymphocytic leukemia. *Blood* 117, 563–574. <https://doi.org/10.1182/blood-2010-05-284984>.
25. Amit, I., Citri, A., Shay, T., Lu, Y., Katz, M., Zhang, F., Tarcic, G., Siwak, D., Lahad, J., Jacob-Hirsch, J., et al. (2007). A module of negative feedback regulators defines growth factor signaling. *Nat. Genet.* 39, 503–512. <https://doi.org/10.1038/ng1987>.
26. Saito, T., and Yamasaki, S. (2003). Negative feedback of T cell activation through inhibitory adapters and costimulatory receptors. *Immunol. Rev.* 192, 143–160. <https://doi.org/10.1034/j.1600-065x.2003.00022.x>.
27. Bhalla, U.S., Ram, P.T., and Iyengar, R. (2002). MAP kinase phosphatase as a locus of flexibility in a mitogen-activated protein kinase signaling network. *Science* 297, 1018–1023. <https://doi.org/10.1126/science.1068873>.
28. Schleiss, C., Carapito, R., Fornecker, L.M., Muller, L., Paul, N., Tahar, O., Pichot, A., Tavian, M., Nicolae, A., Miquet, L., et al. (2021). Temporal multi-omic modeling reveals a B-cell receptor proliferative program in chronic lymphocytic leukemia. *Leukemia* 35, 1463–1474. <https://doi.org/10.1038/s41375-021-01221-5>.
29. Molina, G., Vogt, A., Bakan, A., Dai, W., Queiroz de Oliveira, P., Znosko, W., Smithgall, T.E., Bahar, I., Lazo, J.S., Day, B.W., and Tsang, M. (2009). Zebrafish chemical screening reveals an inhibitor of Dusp6 that expands cardiac cell lineages. *Nat. Chem. Biol.* 5, 680–687. <https://doi.org/10.1038/nchembio.190>.
30. Mougiakakos, D., Johansson, C.C., Jitschin, R., Böttcher, M., and Kiesel, R. (2011). Increased thioredoxin-1 production in human naturally occurring regulatory T cells confers enhanced tolerance to oxidative stress. *Blood* 117, 857–861. <https://doi.org/10.1182/blood-2010-09-307041>.
31. Bichi, R., Shinton, S.A., Martin, E.S., Koval, A., Calin, G.A., Cesari, R., Russo, G., Hardy, R.R., and Croce, C.M. (2002). Human chronic lymphocytic leukemia modeled in mouse by targeted TCL1 expression. *Proc. Natl. Acad. Sci. USA* 99, 6955–6960. <https://doi.org/10.1073/pnas.102181599>.
32. Chan, L.N., Murakami, M.A., Robinson, M.E., Caeser, R., Sadras, T., Lee, J., Cosgun, K.N., Kume, K., Khairnar, V., Xiao, G., et al. (2020). Signalling

- input from divergent pathways subverts B cell transformation. *Nature* 583, 845–851. <https://doi.org/10.1038/s41586-020-2513-4>.
33. Korotchenko, V.N., Saydmohammed, M., Vollmer, L.L., Bakan, A., Sheetz, K., Debiec, K.T., Greene, K.A., Agliori, C.S., Bahar, I., Day, B.W., et al. (2014). In vivo structure-activity relationship studies support allosteric targeting of a dual specificity phosphatase. *Chembiochem* 15, 1436–1445. <https://doi.org/10.1002/cbic.201402000>.
34. Huertas, P., Cortés-Ledesma, F., Sartori, A.A., Aguilera, A., and Jackson, S.P. (2008). CDK targets Sae2 to control DNA-end resection and homologous recombination. *Nature* 455, 689–692. <https://doi.org/10.1038/nature07215>.
35. Esashi, F., Christ, N., Gannon, J., Liu, Y., Hunt, T., Jasin, M., and West, S.C. (2005). CDK-dependent phosphorylation of BRCA2 as a regulatory mechanism for recombinational repair. *Nature* 434, 598–604. <https://doi.org/10.1038/nature03404>.
36. Olsen, B.B., Wang, S.Y., Svenstrup, T.H., Chen, B.P.C., and Guerra, B. (2012). Protein kinase CK2 localizes to sites of DNA double-strand break regulating the cellular response to DNA damage. *BMC Mol. Biol.* 13, 7. <https://doi.org/10.1186/1471-2199-13-7>.
37. Di Segni, M., Virdia, I., Verdina, A., Amoreo, C.A., Baldari, S., Toietta, G., Diodoro, M.G., Mottolise, M., Sperduti, I., Moretti, F., et al. (2022). HIPK2 Cooperates with KRAS Signaling and Associates with Colorectal Cancer Progression. *Mol. Cancer Res.* 20, 686–698. <https://doi.org/10.1158/1541-7786.MCR-21-0628>.
38. Johnson, G.L., and Lapadat, R. (2002). Mitogen-activated protein kinase pathways mediated by ERK, JNK, and p38 protein kinases. *Science* 298, 1911–1912. <https://doi.org/10.1126/science.1072682>.
39. Sehgal, V., and Ram, P.T. (2013). Network Motifs in JNK Signaling. *Genes Cancer* 4, 409–413. <https://doi.org/10.1177/1947601913507577>.
40. Crassini, K., Stevenson, W.S., Mulligan, S.P., and Best, O.G. (2015). The MEK1/2 inhibitor, MEKi-1, induces cell death in chronic lymphocytic leukemia cells under conditions that mimic the tumor microenvironment and is synergistic with fludarabine. *Leuk. Lymphoma* 56, 3407–3417. <https://doi.org/10.3109/10428194.2015.1032963>.
41. Kelly, D.P., and Scarpulla, R.C. (2004). Transcriptional regulatory circuits controlling mitochondrial biogenesis and function. *Genes Dev.* 18, 357–368. <https://doi.org/10.1101/gad.1177604>.
42. Pyakurel, A., Savoia, C., Hess, D., and Scorrano, L. (2015). Extracellular regulated kinase phosphorylates mitofusin 1 to control mitochondrial morphology and apoptosis. *Mol. Cell* 58, 244–254. <https://doi.org/10.1016/j.molcel.2015.02.021>.
43. Ansari, M.Y., Novak, K., and Haqqi, T.M. (2022). ERK1/2-mediated activation of DRP1 regulates mitochondrial dynamics and apoptosis in chondrocytes. *Osteoarthritis Cartilage* 30, 315–328. <https://doi.org/10.1016/j.joca.2021.11.003>.
44. Dagda, R.K., Zhu, J., Kulich, S.M., and Chu, C.T. (2008). Mitochondrially localized ERK2 regulates mitophagy and autophagic cell stress: implications for Parkinson's disease. *Autophagy* 4, 770–782. <https://doi.org/10.4161/auto.6458>.
45. Balaban, R.S., Nemoto, S., and Finkel, T. (2005). Mitochondria, oxidants, and aging. *Cell* 120, 483–495. <https://doi.org/10.1016/j.cell.2005.02.001>.
46. Campo, E., Cymbalista, F., Ghia, P., Jäger, U., Pospisilova, S., Rosenquist, R., Schuh, A., and Stilgenbauer, S. (2018). TP53 aberrations in chronic lymphocytic leukemia: an overview of the clinical implications of improved diagnostics. *Haematologica* 103, 1956–1968. <https://doi.org/10.3324/haematol.2018.187583>.
47. Döhner, H., Stilgenbauer, S., Benner, A., Leupolt, E., Kröber, A., Bullinger, L., Döhner, K., Bentz, M., and Lichter, P. (2000). Genomic aberrations and survival in chronic lymphocytic leukemia. *N. Engl. J. Med.* 343, 1910–1916. <https://doi.org/10.1056/NEJM200012283432602>.
48. Knittel, G., Liedgens, P., and Reinhardt, H.C. (2015). Targeting ATM-deficient CLL through interference with DNA repair pathways. *Front. Genet.* 6, 207. <https://doi.org/10.3389/fgene.2015.00207>.
49. Prabhakar, S., Asuthkar, S., Lee, W., Chigurupati, S., Zakharian, E., Tsung, A.J., and Velpula, K.K. (2014). Targeting DUSPs in glioblastomas - wielding a double-edged sword? *Cell Biol. Int.* 38, 145–153. <https://doi.org/10.1002/cbin.10201>.
50. Brondello, J.M., Pouyssegur, J., and McKenzie, F.R. (1999). Reduced MAP kinase phosphatase-1 degradation after p42/p44MAPK-dependent phosphorylation. *Science* 286, 2514–2517. <https://doi.org/10.1126/science.286.5449.2514>.
51. Chang, T.S., Cho, C.S., Park, S., Yu, S., Kang, S.W., and Rhee, S.G. (2004). Peroxiredoxin III, a mitochondrion-specific peroxidase, regulates apoptotic signaling by mitochondria. *J. Biol. Chem.* 279, 41975–41984. <https://doi.org/10.1074/jbc.M407707200>.
52. Pabla, N., Ma, Z., McIlhatton, M.A., Fishel, R., and Dong, Z. (2011). hMSH2 recruits ATR to DNA damage sites for activation during DNA damage-induced apoptosis. *J. Biol. Chem.* 286, 10411–10418. <https://doi.org/10.1074/jbc.M110.210989>.
53. Golding, S.E., Rosenberg, E., Neill, S., Dent, P., Povirk, L.F., and Valerie, K. (2007). Extracellular signal-related kinase positively regulates ataxia telangiectasia mutated, homologous recombination repair, and the DNA damage response. *Cancer Res.* 67, 1046–1053. <https://doi.org/10.1158/0008-5472.CAN-06-2371>.
54. Wu, Q.N., Liao, Y.F., Lu, Y.X., Wang, Y., Lu, J.H., Zeng, Z.L., Huang, Q.T., Sheng, H., Yun, J.P., Xie, D., et al. (2018). Pharmacological inhibition of DUSP6 suppresses gastric cancer growth and metastasis and overcomes cisplatin resistance. *Cancer Lett.* 412, 243–255. <https://doi.org/10.1016/j.canlet.2017.10.007>.
55. Scheffold, A., Jebaraj, B.M.C., Tausch, E., Bloehdorn, J., Ghia, P., Yahiaoui, A., Dolnik, A., Blätte, T.J., Bullinger, L., Dheenadayalan, R.P., et al. (2019). IGF1R as druggable target mediating PI3K-delta inhibitor resistance in a murine model of chronic lymphocytic leukemia. *Blood* 134, 534–547. <https://doi.org/10.1182/blood.2018881029>.
56. Zandi, Z., Kashani, B., Alishahi, Z., Pourbagheri-Sigaroodi, A., Esmaeili, F., Ghaffari, S.H., Bashash, D., and Momeny, M. (2022). Dual-specificity phosphatases: therapeutic targets in cancer therapy resistance. *J. Cancer Res. Clin. Oncol.* 148, 57–70. <https://doi.org/10.1007/s00432-021-03874-2>.
57. Wang, Z., Zhou, J.Y., Kanakapalli, D., Buck, S., Wu, G.S., and Ravindranath, Y. (2008). High level of mitogen-activated protein kinase phosphatase-1 expression is associated with cisplatin resistance in osteosarcoma. *Pediatr. Blood Cancer* 51, 754–759. <https://doi.org/10.1002/pbc.21727>.
58. Vicent, S., Garayoa, M., López-Picazo, J.M., Lozano, M.D., Toledo, G., Thunnissen, F.B.J.M., Manzano, R.G., and Montuenga, L.M. (2004). Mitogen-activated protein kinase phosphatase-1 is overexpressed in non-small cell lung cancer and is an independent predictor of outcome in patients. *Clin. Cancer Res.* 10, 3639–3649. <https://doi.org/10.1158/1078-0432.CCR-03-0771>.
59. Gao, Y., Li, H., Han, Q., Li, Y., Wang, T., Huang, C., Mao, Y., Wang, X., Zhang, Q., Tian, J., et al. (2020). Overexpression of DUSP6 enhances chemotherapy-resistance of ovarian epithelial cancer by regulating the ERK signaling pathway. *J. Cancer* 11, 3151–3164. <https://doi.org/10.7150/jca.37267>.
60. Ran, F.A., Hsu, P.D., Wright, J., Agarwala, V., Scott, D.A., and Zhang, F. (2013). Genome engineering using the CRISPR-Cas9 system. *Nat. Protoc.* 8, 2281–2308. <https://doi.org/10.1038/nprot.2013.143>.
61. Doench, J.G., Fusi, N., Sullender, M., Hegde, M., Vaimberg, E.W., Donovan, K.F., Smith, I., Tothova, Z., Wilen, C., Orchard, R., et al. (2016). Optimized sgRNA design to maximize activity and minimize off-target effects of CRISPR-Cas9. *Nat. Biotechnol.* 34, 184–191. <https://doi.org/10.1038/nbt.3437>.
62. Ruprecht, B., Koch, H., Medard, G., Mundt, M., Kuster, B., and Lemeer, S. (2015). Comprehensive and reproducible phosphopeptide enrichment using iron immobilized metal ion affinity chromatography (Fe-IMAC)

- columns. *Mol. Cell. Proteomics* **14**, 205–215. <https://doi.org/10.1074/mcp.M114.043109>.
63. Ruprecht, B., Zecha, J., Zolg, D.P., and Kuster, B. (2017). High pH Reversed-Phase Micro-Columns for Simple, Sensitive, and Efficient Fractionation of Proteome and (TMT labeled) Phosphoproteome Digests. *Methods Mol. Biol.* **1550**, 83–98. [https://doi.org/10.1007/978-1-4939-6747-6\\_8](https://doi.org/10.1007/978-1-4939-6747-6_8).
64. Cox, J., and Mann, M. (2008). MaxQuant enables high peptide identification rates, individualized p.p.b.-range mass accuracies and proteome-wide protein quantification. *Nat. Biotechnol.* **26**, 1367–1372. <https://doi.org/10.1038/nbt.1511>.
65. Tyanova, S., Temu, T., Sinitcyn, P., Carlson, A., Hein, M.Y., Geiger, T., Mann, M., and Cox, J. (2016). The Perseus computational platform for comprehensive analysis of (prote)omics data. *Nat. Methods* **13**, 731–740. <https://doi.org/10.1038/nmeth.3901>.
66. Horn, H., Schoof, E.M., Kim, J., Robin, X., Miller, M.L., Diella, F., Palma, A., Cesareni, G., Jensen, L.J., and Linding, R. (2014). KinomeXplorer: an integrated platform for kinome biology studies. *Nat. Methods* **11**, 603–604. <https://doi.org/10.1038/nmeth.2968>.
67. Raaijmakers, L.M., Giansanti, P., Possik, P.A., Mueller, J., Peeper, D.S., Heck, A.J.R., and Altelaar, A.F.M. (2015). PhosphoPath: Visualization of Phosphosite-centric Dynamics in Temporal Molecular Networks. *J. Proteome Res.* **14**, 4332–4341. <https://doi.org/10.1021/acs.jproteome.5b00529>.
68. Szklarczyk, D., Gable, A.L., Lyon, D., Junge, A., Wyder, S., Huerta-Cepas, J., Simonovic, M., Doncheva, N.T., Morris, J.H., Bork, P., et al. (2019). STRING v11: protein-protein association networks with increased coverage, supporting functional discovery in genome-wide experimental datasets. *Nucleic Acids Res.* **47**, D607–D613. <https://doi.org/10.1093/nar/gky1131>.
69. Slenter, D.N., Kutmon, M., Hanspers, K., Riutta, A., Windsor, J., Nunes, N., Mélius, J., Cirillo, E., Coort, S.L., Digles, D., et al. (2018). WikiPathways: a multifaceted pathway database bridging metabolomics to other omics research. *Nucleic Acids Res.* **46**, D661–D667. <https://doi.org/10.1093/nar/gkx1064>.
70. Parekh, S., Ziegenhain, C., Vieth, B., Enard, W., and Hellmann, I. (2016). The impact of amplification on differential expression analyses by RNA-seq. *Sci. Rep.* **6**, 25533. <https://doi.org/10.1038/srep25533>.
71. Macosko, E.Z., Basu, A., Satija, R., Nemesh, J., Shekhar, K., Goldman, M., Tirosh, I., Bialas, A.R., Kamitaki, N., Martersteck, E.M., et al. (2015). Highly Parallel Genome-wide Expression Profiling of Individual Cells Using Nanoliter Droplets. *Cell* **161**, 1202–1214. <https://doi.org/10.1016/j.cell.2015.05.002>.

# STAR★METHODS

## KEY RESOURCES TABLE

REAGENT or RESOURCE	SOURCE	IDENTIFIER
<b>Antibodies</b>		
FACS: human anti-CD5 Pe-Cy7 (L17F12)	BioLegend	364008
FACS: human anti-CD19 APC (HIB19)	BioLegend	302212
FACS: human anti-CD19 PE (HIB19)	BioLegend	302208
FACS: human anti-pERK Brilliant Violet 421 (6B8B69)	BioLegend	369509
FACS: human anti-pH2AX PE (20E3)	Cell Signaling Technology	5763S
FACS: human anti-MKP3 (DUSP6) (SR39-09)	Thermo Fisher Scientific	MA5-31988
FACS: mouse anti-CD5 PE (53–7.3)	BioLegend	115530
FACS: mouse anti-CD19 APC-Cy7 (6D5)	BioLegend	100608
WB: anti-ATF2 (20F1)	Cell Signaling Technology	9226
WB: anti-pATF2 (11G2)	Cell Signaling Technology	5112
WB: anti-beta actin (8H10D10)	Cell Signaling Technology	3700
WB: anti-pCHK1 (133D3)	Cell Signaling Technology	2348
WB: anti-DUSP1	Abcam	ab195261
WB: anti-DUSP6	Cell Signaling Technology	3058
WB: anti-pH2AX (20E3)	Cell Signaling Technology	9718
WB: anti-Hsp60	BD Biosciences	611563
WB: anti-p44/42 MAPK (Erk1/2)	Cell Signaling Technology	9102
WB: anti-pp44/42 MAPK (pErk1/2)	Cell Signaling Technology	9101
WB: anti-pSAPK/JNK	Cell Signaling Technology	9251
<b>Biological samples</b>		
Healthy human PBMCs	Bavarian Red Cross, Munich	N/A
CLL patient PBMCs	Munich Clinic Schwabing, Munich	N/A
CLL patient PBMCs	MRI, Munich	N/A
CLL patient PBMCs	National Center for Tumor Diseases, Heidelberg	N/A
<b>Chemicals, peptides, and recombinant proteins</b>		
AZD6672	Selleckchem	S8843
BCI hydrochloride (DUSP1/6 inhibitor)	Axon Medchem	2852
BCI-215 (DUSP1/6 inhibitor)	MedChemExpress	HY-121087
Emricasan (pan-caspase inhibitor)	Selleckchem	S7775
KU-55933 (ATM inhibitor)	Selleckchem	S1092
LY2603618 (CHK1/2 inhibitor)	Cayman Chemical	20351
PD0325901 (MEK1/2 inhibitor)	Selleckchem	S1036
PD98059 (MEK1/2 inhibitor)	Hözel Biotech	HY-12028
QVD (pan-caspase inhibitor)	D Biosciences	563828
SB 202190 (p38 inhibitor)	MedChemExpress	HY-10295
SP600125 (JNK inhibitor)	MedChemExpress	HY-12041
Trametinib (MEK1/2 inhibitor)	Selleckchem	S2673
N-acetylcysteine (NAC, antioxidant)	Thermo Fisher Scientific	C10491
cOmplete™, EDTA-free Protease Inhibitor Cocktail	Roche	04693132001
Phosphatase Inhibitor Cocktail 1	Sigma Aldrich	P2850

(Continued on next page)

**Continued**

REAGENT or RESOURCE	SOURCE	IDENTIFIER
Phosphatase Inhibitor Cocktail 2	Sigma Aldrich	P5726
<b>Critical commercial assays</b>		
Annexin V (APC) Apoptosis Detection Kit	eBioscience	88-8007-72
APC Conjugation Kit	Abcam	ab201807
Pierce™ ECL Western Blotting Substrate	Thermo Fisher Scientific	32106X4
Pierce™ BCA Protein Assay Kit	Thermo Fisher Scientific	23227
MitoSOX™ Red	Thermo Fisher Scientific	M36008
B Cell Isolation Kit II, human	Miltenyi Biotec	130-091-151
Cell Line Nucleofector™ Kit V	Lonza	VCA-1003
PTMScan® PhosphoTyrosine Rabbit mAb (P-Tyr-1000) Kit	Cell Signaling Technology	8803
<b>Deposited data</b>		
Phospho-proteome data login: <a href="mailto:reviewer_pxd032039@ebi.ac.uk">reviewer_pxd032039@ebi.ac.uk</a> PW: DGfgX3Xf	ProteomeXchange Consortium	PXD032039
RNA sequencing data	European Nucleotide Archive (ENA)	PRJEB63405
<b>Experimental models: Cell lines</b>		
Human: MEC-1	DSMZ	DSMZ: ACC 497, RRID: CVCL_1870
Human: OSU-CLL	PMID: 24130782	N/A RRID: CVCL_Y382
Human: EHEB	DSMZ	DSMZ: ACC 67 RRID: CVCL_1194
Human: HBL-1	PMID: 2854303	N/A RRID: CVCL_4213
Human: Jurkat	ATCC	ATCC: TIB-152 RRID: CVCL_0065
Human: HuT-78	ATCC	ATCC: TIB-161 RRID: CVCL_0337
<b>Experimental models: Organisms/strains</b>		
Mouse: C57BL/6J	The Jackson Laboratory	JAX: 000664
Mouse: Tg(Igh-V186.2-TCL1A)3Cro	N/A	MGI:3527221
<b>Oligonucleotides</b>		
All oligonucleotide sequences can be found in <a href="#">Table S2</a>	This study	N/A
<b>Recombinant DNA</b>		
pSpCas9(BB)-2A-GFP (Px458)	Ran et al. <sup>60</sup>	Addgene #48138
<b>Software and algorithms</b>		
ImageJ	PMID: 22930834	<a href="https://imagej.net/ij/download.html">https://imagej.net/ij/download.html</a>
FlowJo™	Becton, Dickinson and Company	<a href="https://www.flowjo.com/solutions/flowjo/downloads">https://www.flowjo.com/solutions/flowjo/downloads</a>
MaxQuant	Max-Planck-Institute of Biochemistry	<a href="https://www.maxquant.org/maxquant/">https://www.maxquant.org/maxquant/</a>
Perseus	Max-Planck-Institute of Biochemistry	<a href="https://maxquant.net/perseus/">https://maxquant.net/perseus/</a>
<b>Other</b>		
Sep-Pak C18 1 cc Vac Cartridge, 50 mg Sorbent per Cartridge, 55–105 μm	Waters	SKU: WAT054955
TMT10plex™ Set	Thermo Fisher Scientific	90110
ProPac IMAC-10 Column (4 × 50 mm)	Thermo Fisher Scientific	063276

## RESOURCE AVAILABILITY

### Lead contact

Information and requests for resources and reagents should be directed to and will be fulfilled by the lead contact, Maike Buchner ([maike.buchner@tum.de](mailto:maike.buchner@tum.de)).

### Materials availability

This study did not generate new unique reagents.

### Data and code availability

Phospho-proteome data have been deposited at ProteomeXchange Consortium and are publicly available as of the date of publication. RNA sequencing data have been deposited in the European Nucleotide Archive (ENA) and are publicly available as of the date of publication. Accession numbers are listed in the [key resources table](#).

This paper does not report original code.

Any additional information required to reanalyze the data reported in this paper is available from the [lead contact](#) upon request.

## EXPERIMENTAL MODEL AND SUBJECT DETAILS

### Mice

For murine *in vivo* experiments, we collected splenocytes from aged TCL1-tg mice<sup>31</sup> (>10 months, male and female) with developed CLL and injected them equally into wt recipient mice to generate comparable experimental groups. To do this, we injected  $2 \times 10^7$  CLL splenocytes i.v. into female littermate C57BL/6 wt immunocompetent mice ( $n = 10$ ) at the age of 8–10 weeks and waited for the detection of murine CLL cells in the peripheral blood (PB). The mice were distributed into one vehicle-treated group (5% DMSO in PBS) and one DUSPi-treated group (10 mg/kg BCI-215) with equal CLL content in the PB with  $n = 5$  each. Treatment was initiated daily for a total of 10 doses in a random order to minimize potential confounders. Thereafter, content of CLL cells in peripheral blood, spleen, or peritoneal cavity in % of viable cells was determined by flow cytometry in both groups. Data are presented as mean values  $\pm$  SD. Statistical significance was assessed by a two-tailed unpaired Student's t-test. Animals would have been excluded if no CLL engraftment would have been detected prior to treatment. No exclusion in our experiments was necessary.

### Cell lines and primary CLL cells

MEC-1 (male, RRID: CVCL\_1870) cells were cultured in IMDM, and OSU-CLL (male, RRID: CVCL\_Y382), EHEB (female, RRID: CVCL\_1194), HUT-78 (male, RRID: CVCL\_0337), HBL-1 (male, RRID: CVCL\_4213), and Jurkat (male, RRID: CVCL\_0065) cells were cultured in RPMI-1640 medium supplemented with 10% FBS and 1% Pen-Strep (100U/mL penicillin, 100  $\mu$ g/mL streptomycin), and cultured at 37°C, 5% CO<sub>2</sub>.

Primary CLL samples were isolated from the peripheral blood of male and female patients treated at the Klinikum rechts der Isar, München Klinik Schwabing, or the National Center for Tumor Diseases, Heidelberg ([Table S1](#)). Patient sampling was approved by the local ethics committee, and informed consent was obtained from all patients. Healthy donor-derived blood samples were obtained from Bavarian Red Cross (Munich, Germany). Primary CLL cells were cultured in RPMI-1640 medium supplemented with 10% FBS and 1% Pen-Strep (100U/mL penicillin, 100  $\mu$ g/mL streptomycin), 1% HEPES (10 mM), 1% MEM NEAA (1X), and 1% sodium pyruvate (1 mM). The cells were cultured at 37°C, 5% CO<sub>2</sub>. Patient samples were anonymized for the experimental use, we did not see an influence of the patient's sex.

## METHOD DETAILS

### Inhibitor treatment and subsequent analysis

Primary patient-derived CLL cells, MEC-1 cells, B- and T cell lymphoma, or healthy peripheral blood MACS-isolated B-cells were seeded at 200,000 cells/well in 96-well-plates or 500,000 cells in 24-well plates and treated with BCI alone or in combination with the indicated inhibitors. Viability was analyzed by flow cytometry.

### Generating DUSP1 and DUSP6 knock outs

Target guide oligonucleotides<sup>61</sup> ([Table S2](#)) were ordered from Eurofins. To clone respective sequences into vector Px458,<sup>60</sup> following strategy was applied.

### Oligo annealing and phosphorylation

Pipetting scheme: 0.5  $\mu$ L fwd Primer (100  $\mu$ M), 0.5  $\mu$ L rev Primer (100  $\mu$ M), 0.5  $\mu$ L T4 Ligation Buffer (10x), 0.5  $\mu$ L T4 Kinase, 3  $\mu$ L H<sub>2</sub>O.  
Program: 37°C for 30 min–95°C for 5 min – cool down until 25°C – hold at 8°C.

### Golden gate cloning

Pipetting scheme: 0.5  $\mu$ L vector (Px458) (100 ng), 1  $\mu$ L Oligos (diluted 1:200), 1  $\mu$ L Tango Buffer (10x), 0.5  $\mu$ L DTT (10mM), 0.5  $\mu$ L ATP (10mM) 0.5  $\mu$ L FD Bpil, 0.5  $\mu$ L T4 ligase, 5.5  $\mu$ L H<sub>2</sub>O.

Program: 37°C for 5 min–21°C for 5 min - 6 cycles, hold at 8°C.

### Plasmid safe ligation

Pipetting scheme: 5.5  $\mu$ L Golden Gate Cloning Ligation, 0.75  $\mu$ L Plasmid Safe Buffer (10x), 0.75  $\mu$ L ATP (10mM), 0.5  $\mu$ L PlasmidSafe exonuclease.

Program: 37°C for 30 min - 70°C for 30 min - hold at 8°C.

### Nucleofection-based transient transfection

For transient transfection of the Cas9 plasmid (Px458) containing the sgRNAs, the Amaxa nucleofection (Lonza Bioscience) system was applied, according to manufacturer's instructions. Amaxa Nucleofector Kit V was applied and  $2 \times 10^6$  MEC-1 cells were transfected with 5–20  $\mu$ g plasmid by application of the program X-001. 48 h post transfection, cells were sorted for GFP expression.

### Retroviral CRISPR knockout generation

Alternatively, we used retroviral CRISPR approaches to generate DUSP knockout MEC-1 cells. For this, MEC-1 Eco cells were transduced with DUSP-targeting guide RNAs (sgRNAs, Table S2) and pMIG-Cas9 containing retrovirus. After 48 h from transduction cells were selected with 1  $\mu$ g/ml of puromycin for 3 days. The selected cells were seeded as single colonies in 96-well plates by FACS sorting. After 3–4 weeks of culture, cells derived from each colony were used to assess DUSP knockout by western blotting and genomic sequencing of the sgRNA target region.

In order to validate successfully generated CRIPR/Cas9 knockouts in MEC-1 cells, DNA was isolated from  $2 \times 10^6$  cells and forward and reverse amplification primer (Table S2) spanning the respective Cas9 targeted sequences were applied in the following PCR reaction.

### Pipetting scheme

50–100 ng template, 10  $\mu$ L HF Buffer (5x), 2  $\mu$ L dNTPs (2.5 mM), 1  $\mu$ L DMSO, 1  $\mu$ L Primer forward, 1  $\mu$ L Primer reverse, 1  $\mu$ L Phusion Polymerase, H<sub>2</sub>O (in total 50  $\mu$ L reaction)

### Programm

98°C for 45 s.

98°C for 20 s - 72°C for 2.5 min - 5 cycles.

98°C for 20 s - 68°C for 30 s - 72°C for 2.5 min - 5 cycles.

98°C for 20 s - 65°C for 30 s - 72°C 2.5 min - 5 cycles.

72°C for 5 min.

Upon PCR, the amplified reactions were loaded on 2% agarose gels and respective amplified DNA sequences were isolated, purified and sent for sequencing with respective sequencing primers (Table S2). For sequencing of DUSP1 amplified DNA, primers spanning Exon 1 (targeted by guide 1, 2, 4) and Exon 2 (targeted by guide 3) were applied. For sequencing of DUSP6 amplified DNA, primers spanning Exon 1 (targeted by all guides) were used.

### Immunoblot

For immunoblots, cell lysates were prepared by washing cell pellets twice with PBS, followed by incubation in RIPA buffer supplemented with EDTA-free protease inhibitor cocktail (Roche) and phosphatase inhibitors (Sigma Aldrich) for 15 min on ice, and centrifugation for 15 min at full speed at 4°C. Total protein concentration was determined using a Bradford assay. The samples were prepared with 6x Lämmli loading buffer and heat denaturated at 95°C for 5 min and separated with a 10% SDS-PAGE. The proteins were transferred onto nitrocellulose membranes. The membranes were blocked with 5% BSA in TBST for 30 min before incubating with primary antibody overnight at 4°C. The membranes were washed with TBST three times for 10 min each, before incubation with the secondary antibody at RT for 1 h. The membranes were analyzed with ECL Western Blotting Substrate (Thermo) using Bio-Rad's ChemiDoc System.

### Competition assay

We applied competition assays to study the growth behavior of generated DUSP1 and DUSP6 knockouts in MEC-1 cells.  $5 \times 10^5$  knockout cells of 2 independent clones, respectively, that were GFP-positive, were mixed with equal amounts of MEC-1 wildtype, GFP-negative cells, or vice versa. The percentage of GFP over time was followed by flow cytometric analysis.

### AnnexinV staining

Primary human CLL cells were treated with BCI for 24 h or 48 h. Cells were washed once in PBS and then in Annexin-V (AnxV) Binding Buffer, diluted 1:10 in sterile water (400x g, 4°C, 5 min). AnxV (APC) was diluted 1:40 in AnxV Binding Buffer and 20  $\mu$ L were applied

per sample, for 15 min at room temperature, protected from light. Afterward, 50  $\mu$ L AnxV Binding buffer, supplemented with 1:1000 diluted DAPI (1 mg/mL), were added and cells were characterized as viable (AnxV<sup>-</sup>, DAPI<sup>-</sup>), apoptotic (AnxV<sup>+</sup>, DAPI<sup>-</sup>), late apoptotic (AnxV<sup>+</sup>, DAPI<sup>+</sup>) and necrotic cells (AnxV<sup>-</sup>, DAPI<sup>+</sup>) by flow cytometry.

### Phospho-proteome screen

Freshly isolated primary CLL cells were treated with BCI for 3 and 10 min; MEC-1 cells were incubated for 24 h at a cell density of  $1 \times 10^6$ /mL and then treated with BCI for 15 and 45 min before isolating protein. Cells were lysed in 8 M urea, 40 mM Tris-HCl pH 8, in the presence of EDTA-free protease inhibitor cocktail (Roche) and phosphatase inhibitors mixture consisting of Phosphatase inhibitor cocktail 1 and 2 (Sigma Aldrich) at  $1\times$  and  $5\times$  of the final concentration, as recommended by the manufacturer. Lysates were then sonicated with a Bioruptor Plus (Diagenode) for 10 cycles of 30 s and cleared by centrifugation for 10 min at 20,000 g and 4°C. Subsequently, total protein concentration was determined using a Bradford assay. Protein lysates, (200  $\mu$ g for CLL cells, 1 mg for MEC-1 cells) were reduced with 10 mM DTT at 37°C for 40 min on a thermoshaker at 700 rpm, and alkylated with 55 mM 2-chloroacetamide at room temperature for 30 min in the dark. Proteins were digested overnight at 37°C with sequencing grade modified trypsin (1:100 enzyme-to-substrate ratio) after 4-fold dilution with 40 mM Tris-HCl, pH 7.6. Digests were acidified by addition of formic acid (FA) to 5% (v/v), and after centrifugation for 5 min at 10,000  $\times$ g, desalting of the peptide solution supernatant was performed using Sep-Pak C18 cartridges and a vacuum manifold according to the manufacturer's instructions. Sep-Pak eluate was frozen at  $-80^\circ\text{C}$  and dried *in vacuo*.

### TMT labeling

TMT 10-plex labeling (9 channels) was performed by reconstituting 200  $\mu$ g of each digest in 20  $\mu$ L of 50 mM HEPES (pH 8.5). 5  $\mu$ L of 11.6 mM TMT reagents stock solution (Thermo) in 100% anhydrous ACN were then added to each sample. Labeling reaction was carried for 1 h at 20°C on a thermoshaker at 400 rpm, and quenched by adding 2  $\mu$ L of 5% hydroxylamine. Peptide solutions were pooled and acidified using 20  $\mu$ L of 10% FA. Reaction vessels in which the labeling took place were further rinsed with 20  $\mu$ L of 10% FA in 10% ACN, and the solvent was then added to the pooled sample. The pools were dried *in vacuo*, desalted and stored dried at  $-80^\circ\text{C}$  until further use.

### Phospho-peptide enrichment and fractionation

Phospho-peptide enrichment was performed by loading the TMT-labeled peptides on a  $\text{Fe}^{3+}$ -IMAC column (Propac IMAC-10 4  $\times$  50 mm column, Thermo).<sup>62</sup> The eluate of the IMAC enrichment was desalted and subjected to high pH RP fractionation<sup>63</sup> using self-packed StageTips, containing 5 disks of C18 material (3 M Empore). For the global phospho-proteome analysis, a total of 6 fractions were collected, dried *in vacuo* and stored at  $-20^\circ\text{C}$  until LC-MS/MS analysis. For phospho-tyrosine analysis, the TMT-labeled peptides were subjected to antibody-based enrichment using the PTMScan PhosphoTyrosine Rabbit mAb (P-Tyr-1000, Cell Signaling Technology) kit, according to the manufactures' recommendations. Briefly, dried peptides were resuspended in 1.4 mL of IP buffer (50 mM MOPS, pH 7.2, 10 mM sodium phosphate, and 50 mM NaCl). The labeled peptide mixture was added to 80  $\mu$ L of P-Tyr-1000 antibody beads, and incubation was performed overnight at 4°C with gentle shaking. Beads were washed two times with 1 mL IP buffer and four times with 1 mL MQ-water, all at 4°C. Peptides were eluted by the addition of 0.15% TFA for 20 min at room temperature. Eluted peptides were desalted on stop-and-go extraction tips and stored at  $-20^\circ\text{C}$  until LC-MS/MS analysis.

### LC-MS/MS analysis

Nano flow LC-ESI-MS measurements were performed using either a Dionex Ultimate 3000 UHPLC+ or a nanoLC-Ultra (Eksigent) system coupled to a Q Exactive HF mass spectrometer (Thermo). Peptides were delivered to a trap column (75  $\mu$ m  $\times$  2 cm, packed in-house with 5  $\mu$ m Reprosil C18 resin; Dr. Maisch) and washed using 0.1% FA at a flow rate of 5  $\mu$ L/min for 10 min. Subsequently, peptides were transferred to an analytical column (75  $\mu$ m  $\times$  45 cm, packed in-house with 3  $\mu$ m Reprosil C18 resin, Dr. Maisch) applying a flow rate of 300 nL/min. Peptides were chromatographically separated using a 100 min linear gradient from 6% to 34% solvent B (0.1% FA, 5% DMSO in ACN) in solvent A (0.1% FA in 5% DMSO). The mass spectrometer was operated in a data-dependent acquisition (DDA) to automatically switch between MS and MS/MS. Briefly, survey full-scan MS spectra were recorded in the orbitrap from 360 to 1300 m/z at a resolution of 60K, using an automatic gain control (AGC) target value of  $3e6$  charges and maximum injection time (maxIT) of 10 or 25 ms. For the MS2-based TMT method, MS2 spectra were recorded in the orbitrap at 30K resolution (AGC of  $2 \times 10^5$  charges, maxIT of 50 ms). The 25 most intense precursor were isolated with an isolation window of 1.2 m/z, and subsequently fragmented by HCD at a normalized collision energy of 33%. Dynamic exclusion was set to 35 s.

### Data processing

Peptide and protein identification and quantification was performed using MaxQuant (version 1.5.5.1 or 1.6.0.13) with its built-in search engine Andromeda.<sup>64</sup> Spectra were searched against the UniProtKB database (Human, UP000005640, 75,771 entries including isoforms, downloaded on 01.2018). Enzyme specificity was set to trypsin, and the search included cysteine carbamidomethylation as a fixed modification and N-term-acetylation of protein, oxidation of methionine, and/or phosphorylation of serine, threonine, tyrosine residue (STY) as variable modifications. TMT10 was specified as label within a reporter ion MS2 experiment type. Up to

two missed cleavage sites were allowed. Precursor tolerance was set to 5 ppm, and fragment ion tolerance to 20 ppm. Results were adjusted to 1% false discovery rate at protein, peptide, and site levels.

### Data analysis for phospho-proteome data

Bioinformatic analysis was done in Microsoft Excel, R, and Perseus (version 1.5.5.3 and 1.6.1.1), which is part of the MaxQuant software suite.<sup>65</sup> Both phosphor-proteome datasets (global and pY) were filtered to remove contaminants and decoy identifications, before performing data normalization of the intensity values by median centering, as implemented in Perseus. Phospho-proteome data were further filtered to retain only class I phosphor-sites (i.e., localization probability >0.75). Datasets were filtered to retain only sites that have been quantified in all the 3 biological replica in at least one experimental condition, and missing values were imputed in Perseus using default settings. To identify significantly regulated phosphorylation sites, Student t-test or ANOVA were used, with a permutation-based FDR of 5% and an S0 parameter of 0.1. Unsupervised hierarchical clustering was performed on z-scored site intensities, using Euclidian distance.

Gene ontology (GO) analysis was performed with Perseus software. Categorical annotation was supplied by Gene Ontology biological process, molecular function, and cellular component, and the KEGG pathway database. All annotations were extracted from the UniProt database. The GO terms enrichment was calculated on the basis of a fisher's exact test with a false discovery rate value of 0.05. Upstream kinases responsible for the observed phosphorylation sites were also predicted by using the NetworKIN algorithm,<sup>66</sup> using default settings. Signaling networks were created in Cytoscape using the PhosphoPath plugin<sup>67</sup> and default parameters. High confidence protein-protein interaction data were downloaded from the STRING database,<sup>68</sup> whereas pathways information was retrieved from Wikipathways.<sup>69</sup>

### RNA preparations and RNA sequencing

For RNASeq, viable MEC-1 and EHEB cells treated with the DUSP1/6 inhibitor BCI (2.5  $\mu$ M) for 4 h or vehicle (DMSO) were sorted and RNA was extracted from whole cell lysates via RNeasy Mini Kit (Qiagen, Hilden, Germany). Library preparation for bulk 3'-sequencing of poly(A)-RNA was done as described previously.<sup>70</sup> Briefly, barcoded cDNA of each sample was generated with a Maxima RT polymerase (Thermo Fisher) using oligo-dT primer containing barcodes, unique molecular identifiers (UMIs) and an adapter. 5' ends of the cDNAs were extended by a template switch oligo (TSO) and after pooling of all samples full-length cDNA was amplified with primers binding to the TSO-site and the adapter. cDNA was fragmented and TruSeq-Adapters ligated with the NEBNext Ultra II FS DNA Library Prep Kit for Illumina (NEB) and 3'-end-fragments were finally amplified using primers with Illumina P5 and P7 overhangs. In comparison to Parekh et al. the P5 and P7 sites were exchanged to allow sequencing of the cDNA in read1 and barcodes and UMIs in read2 to achieve a better cluster recognition. The library was sequenced on a NextSeq 500 (Illumina) with 75 cycles for the cDNA in read1 and 16 cycles for the barcodes and UMIs in read2. Data was processed using the published Drop-seq pipeline (v1.0) to generate sample- and gene-wise UMI tables.<sup>71</sup> Reference genome (GRCg6a) was used for alignment. Transcript and gene definitions were used according to the ENSEMBL annotation release 98.

For analysis, gencode gene annotations v28 and the human reference genome GRCh38 were derived from the Gencode homepage (EMBL-EBI). Dropseq tool v1.12<sup>71</sup> was used for mapping raw sequencing data to the reference genome. The resulting UMI filtered count matrix was imported into R v3.4.4. CPM (counts per million) values were calculated for the rawdata and genes having a mean cpm value less than 1 were removed from the dataset. Prior differential expression analysis with DESeq2 v1.18.1 (10.1186/s13059-014-0550-8), dispersion of the data was estimated with a parametric fit using a multiplicative model where patient and genotype are specified as covariates in the model matrix. The Wald test was used for determining differentially regulated genes between genotypes within each individual patient and shrunken log2 fold changes were calculated afterward. A gene was determined as differentially regulated if the absolute apeglm shrunken log2 fold change was at least 1 and the adjusted p value was below 0.01.

GSEA v4.0.3 (<https://doi.org/10.1073/pnas.0506580102>) was performed in the Preranked mode, where the Wald test-statistic was used as ranking metric. All genes for which a test was conducted went into the analysis. Reference genesets from the MsigDB v7.1 (<https://doi.org/10.1093/bioinformatics/btr260>) were used for testing. A pathway was considered to be significantly associated with a genotype if the FDR value was below 0.05. Rlog transformation of the data was performed for visualization and further downstream analysis.

### QUANTIFICATION AND STATISTICAL ANALYSIS

GraphPad Prism 8 was used for data analysis and statistical significance was calculated using unpaired and paired two-tailed Student's t-test, or 1-way ANOVA. Statistically significant differences are indicated in figures with the associated p value. Error bars in figures indicate the standard deviation (SD). Biological replicates are addressed as the number of n. Technical replicates are not shown. Analyses were not performed under specific randomization or blinding protocol.